

RESEARCH ARTICLE

10.1002/2017MS000977

Axisymmetric Initialization of the Atmosphere and Ocean for Idealized Coupled Hurricane Simulations

Altuğ Aksoy^{1,2} , Jun A. Zhang^{1,2}, Bradley W. Klotz^{1,2} , Eric W. Uhlhorn^{2,3}, and Joseph J. Cione^{2,4} 

¹Cooperative Institute for Marine and Atmospheric Studies, University of Miami, Miami, FL, USA, ²Hurricane Research Division, NOAA/AOML, Miami, FL, USA, ³Now at AIR Worldwide, Boston, MA, USA, ⁴Physical Sciences Division, NOAA/ESRL, Boulder, CO, USA

Key Points:

- A new vortex-scale initialization scheme is developed for idealized coupled hurricane simulations
- For the atmosphere, composite hurricane observations are used; for the ocean, regression models with atmospheric variables are utilized
- The importance of storm speed in controlling upper ocean perturbations in the hurricane inner core is demonstrated

Supporting Information:

- Supporting Information S1
- Data Set S1

Correspondence to:

A. Aksoy,
aaksoy@rsmas.miami.edu

Citation:

Aksoy, A., Zhang, J. A., Klotz, B. W., Uhlhorn, E. W., & Cione, J. J. (2017). Axisymmetric initialization of the atmosphere and ocean for idealized coupled hurricane simulations. *Journal of Advances in Modeling Earth Systems*, 9, 2672–2695. <https://doi.org/10.1002/2017MS000977>

Received 14 MAR 2017

Accepted 19 OCT 2017

Accepted article online 27 OCT 2017

Published online 22 NOV 2017

© 2017. The Authors.

This is an open access article under the terms of the Creative Commons Attribution-NonCommercial-NoDerivs License, which permits use and distribution in any medium, provided the original work is properly cited, the use is non-commercial and no modifications or adaptations are made.

Abstract A new vortex-scale initialization scheme is presented for idealized coupled hurricane simulations. The atmospheric scheme involves construction of azimuthally averaged kinematic and thermodynamic initial fields based on historical composite data sets from hurricane reconnaissance aircraft. For ocean initialization, a statistical scheme is proposed to construct regression models among atmospheric and ocean fields in the hurricane inner core. For the numerical model, the Hurricane Weather Research and Forecasting (HWRF) model coupled with a one-dimensional, diffusive ocean model is used with modifications to initialize with the observation-based vortex and to ensure that the storm environment remains approximately steady. The primary goal in these simulations is to obtain steady state hurricanes of category-1 intensity with characteristics typically observed during the hurricane season of the western Atlantic and Caribbean Sea regions. It is demonstrated that this is successfully achieved in the simulations. In an azimuthally averaged sense, regression models are found to capture about 70% of total variance for sea-surface temperature cooling and up to 55% of total variance for mixed-layer depth perturbation in the hurricane inner core. Furthermore, within the inner core of a hurricane vortex, it is found that storm speed contributes most to upper ocean perturbations, whereas characteristics of the atmospheric vortex contribute very little. The importance of storm speed in controlling upper ocean perturbations is strongest near the storm center, diminishing gradually toward no measurable impact beyond the immediate inner core.

1. Introduction

Hurricanes are complex atmospheric phenomena that manifest fluid motions on a range of spatial scales from microscale turbulence to synoptic-scale environmental flow (Rogers et al., 2013a). This complexity is rendered even more pronounced because the processes that control the development, maintenance, and intensification of hurricanes critically depend on the exchange of energy through the ocean-atmosphere interface (e.g., Bryan, 2012; Bryan & Rotunno, 2009a; Cione et al., 2013; Emanuel, 1995). As a result, investigation of the structure and behavior of hurricanes through both observational and numerical studies has been very challenging, often accomplished by focusing on particular scales of atmospheric motion or particular characteristics of hurricane structure (e.g., Bryan & Rotunno, 2009b; Nolan et al., 2009; Zhang, 2010; Zhang & Drennan, 2012).

Idealized simulations are one such class of hurricane numerical studies that entail many simplifications to the prescription of the storm environment as well as dynamical processes that control hurricane formation and propagation. Such simplifications enable investigators to simulate “cleanly” the impacts of only a limited number of controllable factors on storm structure and behavior. This simplification is in contrast to real-data cases where the evolution of a storm is influenced simultaneously by many factors that are difficult to quantify and constantly changing, cumulatively and nonlinearly contributing to the complexity of isolating the effects of a particular feature that is to be studied. A common type of simplification encountered in idealized simulations is in the form of horizontally uniform atmospheric environments, into which simulated storms are embedded, often ignoring or simplifying the representation of vertical wind shear (shear for brevity hereafter) that impacts most observed hurricanes (e.g., Frank & Ritchie, 1999, 2001; Nguyen et al., 2008, Rappin & Nolan, 2012; D.-L. Zhang et al., 2015; Zhang & Tao, 2013). Another common practice in idealized simulations is to initialize vortices that are analytic solutions of kinematic and mass fields based on various assumptions of balance and to subsequently allow the vortex to evolve and reach equilibrium with the

atmospheric environment in which it is embedded. Some examples for such analytic descriptions of initial vortices can be found in Wang (1995), Nolan and Montgomery (2000), Nolan et al. (2007), Bao et al. (2012), and Zhang and Tao (2013).

When the simplifications involved are sufficiently severe, it has been argued in the literature that hurricanes simulated in idealized studies cannot be verified against observations (e.g., D.-L. Zhang et al., 2015). This is a reasonable corollary considering that no idealized simulation is initialized with an actual observed vortex structure or embedded in an actual observed storm environment: the nonlinear storm evolution that ensues cannot be expected to resemble any actual storm that has been observed. We argue here that idealized studies are nevertheless useful because numerical models in general are capable of representing truthfully the kinematic and thermodynamic processes within hurricanes, therefore rendering realistic model climatologies. We further note that our approach here should not be compared to realistic hurricane simulations with the specific purpose of matching observations as much as possible, such as the nature run in Nolan et al. (2013).

Subject to the above-discussed simplifications in general, it is acknowledged upfront that such verification cannot be carried out against any single observed hurricane. Yet because the model climatology of hurricanes is expected to be accurate relative to observations, verification in a climatological sense must nevertheless be possible. The approach taken here is, then, to initialize the simulation with an observed vortex structure that is climatologically derived and to embed it in a storm environment that is consistent with the climatology of this initial vortex. By further limiting the observations to the climatology of steady state hurricanes, it is expected that, at least in the short range, the state of the simulated hurricane vortex remains generally balanced (i.e., not undergoing rapid changes) so that it can be verified against the very observations that constituted its initial climatological vortex structure and environment. The steady state requirement here is to allow for the application of a static storm environment, a necessary numerical simplification. Although this reduces the degree of complexity achieved in the idealized simulations, realism is not compromised because steady state hurricanes are commonly observed in the nature.

In the present study, the goal is to formulate an initialization scheme for an idealized hurricane model that can provide a realistic vortex structure. For the numerical model, the Hurricane Weather Research and Forecasting (HWRF) model (Bao et al., 2012; Gopalakrishnan et al., 2011, 2013) coupled with a one-dimensional diffusive ocean model (Halliwell et al., 2015) is used with modifications to initialize with the observation-based vortex and to ensure that the storm environment remains steady. To maintain a steady state hurricane during simulations, storm environments climatologically consistent with the observed storm characteristics are applied.

As was demonstrated observationally by Cione and Uhlhorn (2003), sea-surface temperature (SST) cooling in the hurricane inner core is critically linked to intensity change. Here it should be noted that there is no clear-cut definition of the hurricane “inner core” in the literature. Some studies define it by absolute radial distance (e.g., 60 km in Cione & Uhlhorn, 2003 and 200 km in Rogers et al., 2015), while some studies define it relative to the radius of maximum wind (RMW; e.g., 2 RMW in Uhlhorn et al., 2014). In the present study, the convention of Uhlhorn et al. (2014) is followed; i.e., the hurricane inner core is defined as the region within a distance of 2 RMW. To realistically mimic the interactions of the model lower boundary with the underlying ocean through the simulation of SST cooling in the hurricane inner core and its wake, HWRF is coupled with a one-dimensional, diffusive ocean model as in Halliwell et al. (2015). A statistical initialization scheme is then developed that utilizes the correlations among atmospheric and ocean fields to obtain a vortex-scale ocean structure within the initial hurricane inner core.

A primary underlying target with these idealized simulations is to obtain steady state hurricanes of Saffir-Simpson category-1 intensity. The definition of steady state to be followed is that of Rogers et al. (2013b): a hurricane is assumed to be in steady state if the corresponding intensification rate is between -10 and 10 $\text{kt} (24 \text{ h})^{-1}$ ($1 \text{ kt} = 0.5144 \text{ m s}^{-1}$), where intensity is taken from the National Hurricane Center Best Track database and is a subjectively smoothed estimate of the maximum 1 min average wind associated with the tropical cyclone at an elevation of 10 m with an unobstructed exposure at 5 kt precision and 6 h availability (Landsea & Franklin, 2013).

It should be further noted that the definition of a steady state hurricane here is considerably different than the concept of “statistical equilibrium” discussed by Hakim (2011), who introduced model modifications to

simulate storms that are in equilibrium for nearly 500 days. Conversely, Smith et al. (2014) question whether a “globally steady” tropical cyclone can be expected to exist theoretically, on the grounds of the necessity to maintain budgets of angular momentum, heat, and moisture for durations of weeks to months. They argue that, in the absence of steady sources to maintain such budgets, tropical cyclones must be “globally transient.” The concept of steady state in the present study has followed suit and the notion that, observationally, hurricanes are transient dynamical phenomena, thus focusing on much shorter time scales when a hurricane can actually be observed in a steady state. Our simulations indicated that this was indeed the case within a period of ~2 days.

The manuscript is structured as follows: in section 2, the climatological atmospheric and oceanic storm environments are presented first, followed by the description of the idealized HWRF model and ocean coupling. Section 3 focuses on the methodology used to obtain the observation-based initial vortex structure. In section 4, a brief overview of the intensity and intensification rate in simulations is provided to investigate whether steady state hurricanes are successfully simulated. Section 5 describes the statistical approach to obtaining the initial vortex structure of the ocean. To conclude, a summary of results is presented in section 6 with a discussion of relevance, limitations, and future directions.

2. Model Description

The overall modeling methodology is described schematically in Figure 1 and detailed below. A complete end-to-end system is designed with the goal of ensuring that the prescribed atmospheric and ocean environments are consistent with the observation-based initial vortex (i.e., all historical observations of vortex structure and storm environment are chosen to represent category-1, steady state hurricanes observed in

the western tropical Atlantic basin under moderate shear). To obtain a simulation that is minimally impacted by the lateral boundaries for as long as possible, it is carried out on the *f*-plane to eliminate beta drift (Smith, 1993) and the environmental wind profile is adjusted to yield zero mean mass transport so that the simulated storm remains near the domain center. For a realistic interaction with the ocean, the atmospheric model is interfaced with a one-dimensional ocean model that provides cooling in the hurricane core. The details of the modeling framework are explained below.

2.1. Atmospheric Model: Idealized HWRF

The idealized version of HWRF is described in detail in Gopalakrishnan et al. (2011, 2013). However, several differences exist between the versions used in these studies and the present one. These differences are noted in Table 1, along with the specifics about the model. Briefly, three nested computational domains are used at the grid spacing of 27, 9, and 3 km, respectively, with the inner two nests centered on and following the simulated storm center during integration. The innermost nest size is 10° × 10° horizontally to ensure proper transition of the observation-based vortex to the environment. Vertically, a hybrid pressure coordinate system is used with a total of 42 vertical levels and a model top of 50 hPa. The planetary boundary layer (PBL; defined here as the layer between the surface and 850 hPa) is well resolved with 11 vertical levels below 850 hPa. The simulations are carried out in an ocean-only domain on an *f*-plane centered at 21°N latitude.

Because the vortex initialization method is a significant difference between the present and previous versions of idealized HWRF, it is important to also note the vortex-specific parameters that define its structure. Table 2 compares the details of the two versions. The most significant difference is that, here an observation-based vortex of category-1 hurricane intensity is used with a moderate radius of

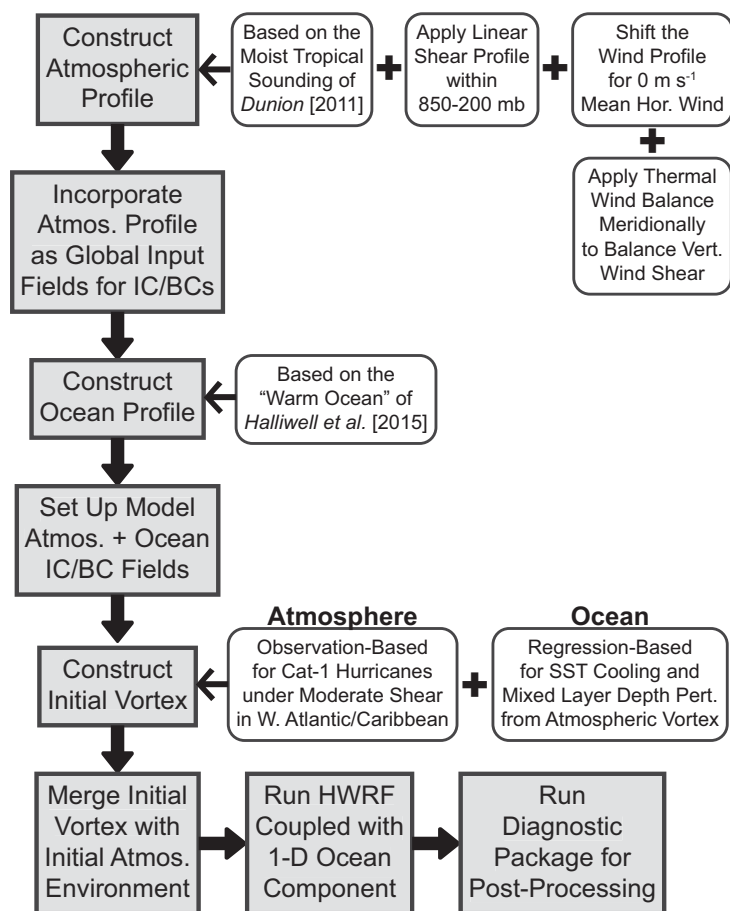


Figure 1. Schematic of the idealized hurricane model initialization and integration.

Table 1
Idealized HWRF Specifics Used in Gopalakrishnan et al. (2013; Left Column) and Those Used in the Present Study (Right Column)

Characteristic	Gopalakrishnan et al. (2013)	Present study
HWRF version	3.2	3.2
Number of computational domains	3	3
Computational domain size (grid spacing)	50° × 50°; 15° × 15°; 5° × 5° (27 km; 9 km; 3 km)	50° × 50°; 15° × 15°; 10° × 10° (27 km; 9 km; 3 km)
Vertical levels	42 hybrid	42 hybrid
Dynamical core	Nonhydrostatic Mesoscale Model (NMM)	NMM
Physics scheme	Ferrier ^a	Ferrier
Cumulus scheme	Simplified Arakawa-Schubert (SAS ^{b,c} ; only outer 2 nests)	SAS (outer 2 nests)
Surface-layer scheme	Roughness length function ^d	Roughness length function
Radiation scheme	Geophysical Fluid Dynamics Laboratory (GFDL) ^e version	GFDL
Ocean coupling (ocean model)	No (n/a)	Yes (1-d diffusive)^f
Initial storm environment (vertical wind shear)	Based on Jordan (1958) (No)	Based on Dunion (2011) (8 m s⁻¹ zonal with thermal wind balancing)
Lateral boundary conditions	Prescribed from GFS	Prescribed consistently with storm environment with zero boundary tendencies
Observation-based initial vortex (atmosphere)	No	Yes
Vortex-scale ocean initialization	No	Yes

Note. Differences are highlighted in bold.

^aFerrier et al. (2002).

^bPan and Wu (1995).

^cHong and Pan (1998).

^dHaus et al. (2010).

^eBender et al. (2007).

^fHalliwell et al. (2015).

maximum wind (RMW) while the Bao et al. (2012) vortex is initialized as a tropical depression with much larger RMW. The simulation of the latter vortex is expected to take one day or longer to spin up and reach a similar strength of the observation-based vortex, ostensibly undergoing a nonlinear evolution in the process, which is nontrivial in terms of both the temporal extent of the simulation and the detailed three-dimensional structure obtained. An initial vortex that already represents some of the main features of observed steady state, category-1 hurricanes is therefore preferable, as it is expected to reduce the magnitude of changes while the model solution converges to steady state. The severity of such changes would, nevertheless, still depend on the realism of the initial vortex in the first place.

2.2. Ocean Coupling: One-Dimensional Ocean Model

The details of the one-dimensional ocean model can be found in Halliwell et al. (2015). Briefly, the momentum equations represent inertial effects horizontally and turbulent diffusion vertically, whereas temperature and salinity are only varied through vertical diffusion. Surface boundary conditions for momentum flux are provided directly by the atmospheric model, where 10 m wind speed, atmospheric temperature, and atmospheric humidity are used to quantify the latent and sensible components of the enthalpy flux through bulk formulas. For mass flux, the atmospheric model provides the precipitation information while evaporation is calculated using a bulk formula. In return, the ocean model provides the SST as the lower boundary condition to the atmospheric model.

It should be noted that, although the one-dimensional ocean model does not reproduce important three-dimensional processes such as

Table 2
Initial Vortex Parameters Provided in Bao et al. (2012; Left Column) and Those Used in the Present Study (Right Column)

	Bao et al. (2012)	Present study
Effective translation speed (m s ⁻¹)	4.0	5.0
Translation direction (° relative to North)	-90	-90
Moving medium	Atmosphere	Ocean
Center latitude (°N)	15.0	21.0
Maximum 10 m wind speed (m s ⁻¹)	20.0	43.7
Radius of maximum wind (km)	90.0	45.0

Note. The row labeled "moving medium" refers to the particular medium (i.e., ocean or atmosphere) that provides the ocean-relative motion of the storm.

upwelling, Halliwell et al. (2015) demonstrate that it does produce a cold wake near the inner core of the hurricane that is sufficiently realistic to characterize model sensitivity to ocean cooling and identify key processes that control this sensitivity.

2.3. Climatological Storm Environment

2.3.1. Atmospheric Environment

The mean atmospheric environment of the simulated storm is obtained from the Dunion (2011) moist tropical sounding, which directly provides the first-guess profiles of temperature and relative humidity. Meanwhile, an idealized wind profile is constructed as follows (the final pressure and temperature profiles are also adjusted to achieve thermal wind balance):

1. Winds are only allowed to vary in the zonal direction and the meridional wind speed is set to zero at all vertical levels.
2. The zonal wind speed profile contains a constant negative (easterly) value in the PBL to mimic the generally easterly low-level flow in the Dunion (2011) wind sounding.
3. Westerly (increasing in zonal direction) shear of 8 m s^{-1} with a linear profile is added between the layers of 850 and 200 hPa. This shear value is consistent with the Dunion (2011) sounding.
4. The zonal wind speed above 200 hPa is constant.
5. The entire wind profile is shifted (thereby maintaining the relative 850–200 hPa shear magnitude) by adjusting the PBL wind speed so that the resulting mass-weighted average zonal wind speed \bar{u} is zero as in

$$\bar{u} = \frac{\sum_k \bar{u}_k \cdot \bar{\rho}_k \cdot \Delta p_k}{\sum_k \bar{\rho}_k \cdot \Delta p_k} = 0, \quad (1)$$

where k is vertical level, ρ is air density, p is pressure, Δ stands for layer difference, overbar denotes layer average, and all local operations involve two adjacent vertical levels. This shifting of the wind profile aims to arrive to a mean atmospheric storm motion speed that is $\sim 0 \text{ m s}^{-1}$ during the simulation, so that the simulated storm generally remains near the center of the model domain. Ocean-relative storm motion is ultimately obtained by moving the ocean zonally at a specified speed instead, as explained further below.

6. The resulting atmospheric profiles of zonal wind, relative humidity, temperature, and dew-point temperature along the storm center latitude are shown in Figures 2a and 2b.
7. Due to the presence of zonal wind shear, the environmental mass fields need to be adjusted meridionally to obtain thermal wind balance. This adjustment is achieved by following the iterative procedure described in the appendix of Nolan (2011). Briefly, the vertical pressure profile p_{ctr} at the center latitude is computed through vertical integration of the hydrostatic equation by

$$p_{ctr}^{k+1} = p_{ctr}^k \cdot \exp\left(-\frac{g}{RT_v} \Delta z\right), \quad (2)$$

where k denotes the vertical index, g is the acceleration of gravity, R is the dry gas constant, z is geopotential height, and T_v is virtual temperature calculated from temperature (T) and specific humidity (q) using

$$T_v = T(1 + 0.608q). \quad (3)$$

The pressure and temperature profiles are then adjusted latitudinally within a range of $\pm 50^\circ$ from center latitude to obtain geostrophic balance with the zonal wind profile integrating the geostrophic balance equation:

$$\frac{\partial p}{\partial y} = -\rho f u = -\frac{p}{RT_v} f u, \quad (4)$$

where y is latitude and the Coriolis parameter f is constant (the f -plane). This procedure is repeated on each vertical level using a Crank-Nicholson semiimplicit scheme by

$$p_{j+1}^k = p_j^k \left(\frac{1 - \Delta y a_j^k / 2}{1 + \Delta y a_j^k / 2} \right), \quad (5)$$

where j denotes the latitude index and

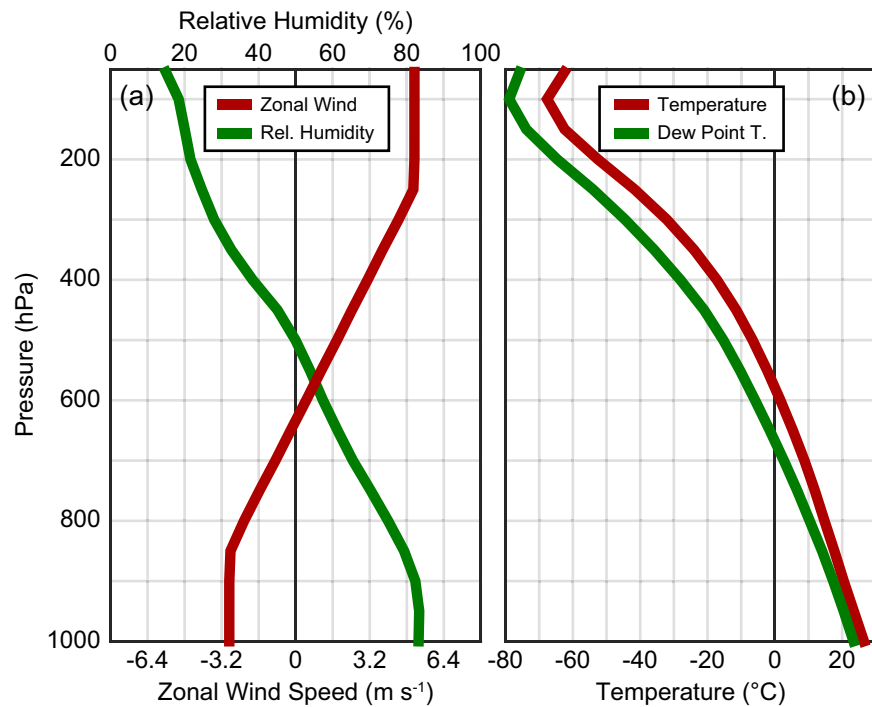


Figure 2. Specification of the atmospheric environment. (a) Zonal wind speed (m s^{-1} , red) and relative humidity (% , green). (b) temperature ($^{\circ}\text{C}$, red) and dew-point temperature ($^{\circ}\text{C}$, green).

$$a_j^k = \frac{f u_j^k}{R T_{v,j}^k} \quad (6)$$

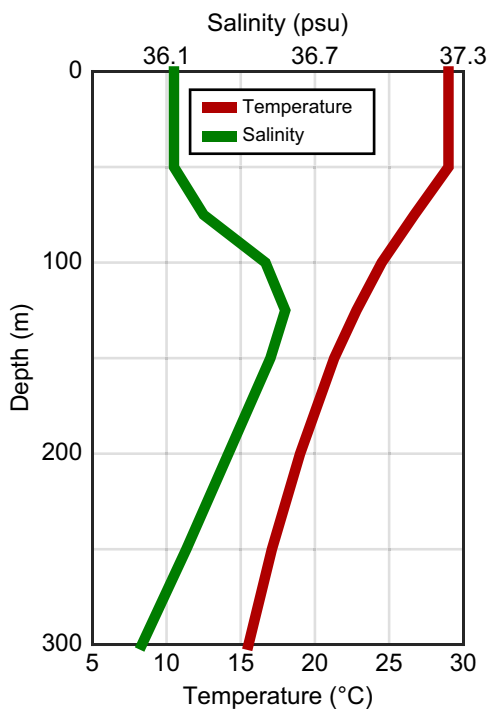


Figure 3. Specification of the ocean environment: temperature ($^{\circ}\text{C}$, red) and salinity (psu, green).

T_v profile is then recalculated using equation (2) to reestablish hydrostatic balance. Equations (4–6) are repeated iteratively until convergence. For the atmospheric storm environment described here, this scheme is able to attain a reduction of domain-wide root-mean-squared difference in T_v and p at a rate of $\sim O(1)$ (iteration) $^{-1}$ in the first 10 iteration steps. The final T profile is then computed by inverting equation (3).

Because HWRF, by design, cannot be integrated using open boundary conditions, a major improvement here upon previous HWRF-based idealized studies (e.g., Bao et al., 2012; Gopalakrishnan et al., 2013; Halliwell et al., 2015) is that the above-described storm environment procedure is applied by overwriting the global fields that contribute to the initial and lateral boundary conditions at all integration times, thereby maintaining unchanging storm environment in the entire computational domain along with consistent static lateral boundary tendencies throughout the simulation. This enables the interior of the simulation domain to remain consistent with its boundaries for a longer period of model integration.

2.3.2. Ocean Environment

The mean ocean environment of the simulated storm is obtained from Halliwell et al. (2015) “warm ocean” specification with an SST of 29°C , which is typical for the western Atlantic warm pool region at the peak of the hurricane season. The tropical cyclone heat potential (e.g., Lin et al. 2013) for this ocean profile is 85 kJ cm^{-2} and the mixed-layer depth (MLD) is 50 m. The corresponding salinity profile peaks at 36.58

psu at 125 m depth. The resulting ocean profiles of temperature and salinity are shown in Figure 3. This “warm ocean” profile is applied uniformly throughout the numerical domain at the initial time of the simulation.

3. Vortex-Scale Atmospheric Initialization: An Observation-Based Approach

3.1. Thermodynamic Fields

Objective analyses of pressure, temperature, and humidity are developed from a weighted combination of historical radius-versus-height observation cross sections (Hawkins & Imbembo, 1976; Hawkins & Rubsam, 1968; LaSeur & Hawkins, 1963) and several thousand Global Positioning System dropwindsonde (dropsonde hereafter) profiles from multiple aircraft, both low and high altitude.

The historical analyses serve as a low-weight background and are useful where significant dropsonde data gaps exist, particularly radially within 5 RMW from storm center above 3 km altitude. These analyses are constructed from in situ aircraft measurements taken at several levels throughout the depth of the troposphere in Hurricane Cleo in 1958 at 75 kt intensity (LaSeur & Hawkins, 1963), Hurricane Hilda in 1964 at 90 kt intensity (Hawkins & Rubsam, 1968), and Hurricane Inez in 1966 at 120 kt intensity (Hawkins & Imbembo, 1976). In all three of these cases, the inner-core thermodynamic structure was well sampled, and the height of the upper level warm-core anomaly maximum was identified, which is crucial for establishing a hurricane-like initial vortex. Each of these background analyses are blended in the far field with the Jordan (1958) mean hurricane season tropical atmosphere sounding, modified in the troposphere based on the results of Dunion and Marron (2008), who separated the impact of the Saharan air layer infecting the Jordan mean profile.

As part of a dropsonde database development effort (Zhang & Uhlhorn, 2012), each dropsonde is associated with several storm-specific parameters, including intensity, RMW, and environmental deep-layer shear vector. With the historical analyses serving as a first guess, a Barnes-type successive correction procedure (Barnes, 1964) is used to interpolate the observations to a regular radius-versus-height grid extending radially from 0 to 20 RMW, and vertically from the surface to 20 km altitude. Any given analyzed quantity \hat{a}_k on grid point k is determined by weighting all available observations on grid points i as follows:

$$\hat{a}_k = \frac{\sum_i a_i w_i}{\sum_i w_i}. \quad (7)$$

The weights w_i are determined by a general Gaussian function of the form:

$$w_i = \exp\left(-\sum_j \frac{\delta_{ij}^2}{S_j^2}\right). \quad (8)$$

Here δ_{ij}^2 is the squared distance from the grid point k to the i th observation for the j th parameter, scaled by S_j^2 . The parameters are radial distance, height, intensity, and shear magnitude, with appropriate scales chosen for each. This enables the construction of an analysis for a specified intensity and shear, since dropsonde profiles obtained in storms closer to the chosen intensity and shear are given higher weight. The spatial coverage of the dropsonde data points that are used in the analyses is shown in Figure 4.

3.2. Wind Fields

Observation-based analyses of horizontal wind components (radial V_r and tangential V_t) are developed from the dropsondes and the large database of airborne Doppler-radar-derived three-dimensional wind fields in hurricanes (e.g., Rogers et al., 2013b). Dropsonde data coverage gaps similar to those in the thermodynamic quantities exist for the winds, while the radar is useful for measuring winds in the inner core throughout the depth of the troposphere. However, a conspicuously poorly observed portion of the storm is the outflow layer (above ~ 12 km altitude) well outside the inner core; due to a lack of scatterers, the radar does not typically observe winds in this region, and the dropsonde winds (mainly from the NOAA G-IV aircraft) are limited to below this crucial layer of the atmosphere. To fill in this data void, the objective analysis first guess is obtained from a HWRF Ensemble Data Assimilation System (HEDAS) analysis of Hurricane Earl (2010; Aksoy, 2013; Aksoy et al., 2013) which adequately resolves the complete storm circulation, including the strong radial outflow near the tropopause.

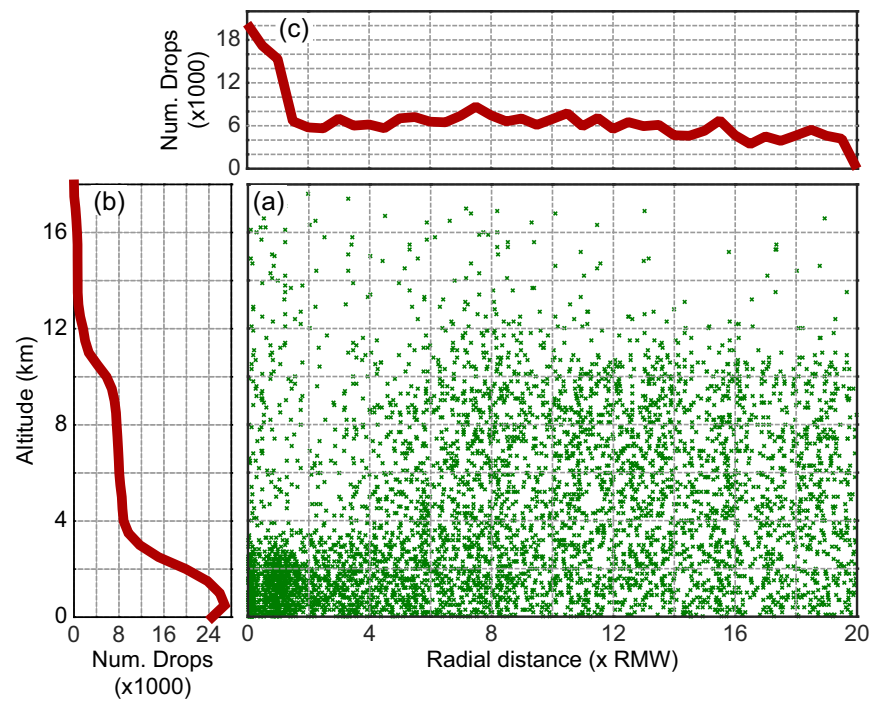


Figure 4. Spatial distribution of historical dropsonde data points used in the construction of observation-based initial vortex. (a) Height-radius scatter diagram of all data points. (b) Number of data points as a function of altitude (km). (c) Number of data points as a function of radius. Radius measures distance from storm center, normalized by RMW.

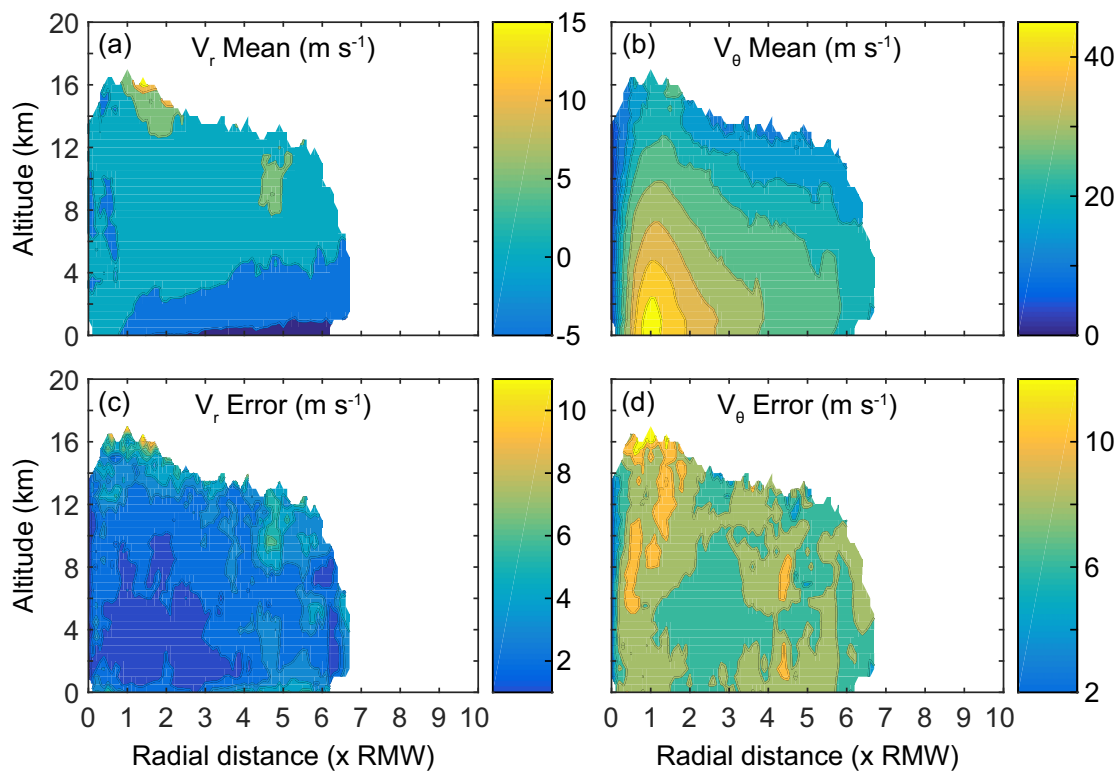


Figure 5. Spatial distribution of azimuthally averaged Doppler radar wind fields used in the construction of observation-based initial vortex. (a) Radial wind speed (V_r ; $m s^{-1}$, negative values indicate flow toward storm center). (b) Tangential wind speed (V_θ ; $m s^{-1}$, positive values indicate cyclonic flow). (c) Radial wind speed error ($m s^{-1}$). (d) Tangential wind speed error ($m s^{-1}$). The errors represent the root-mean-squared residuals of the Barnes-type analysis at each grid point.

The objective analysis procedure for horizontal wind components is otherwise identical to that for the thermodynamic variables. The spatial coverage of the airborne Doppler radar wind fields (an average over 83 individual analyses) that are input to the objective analysis is shown in Figure 5.

4. The Steady State Nature of the Simulations

Before introducing the new ocean initialization methodology, a brief overview of the intensity evolution in the control run is provided. It is noted for clarification that the control run, despite being a coupled atmosphere-ocean simulation, does not include vortex-scale ocean initialization but only the observation-based atmospheric initialization described in the previous section. Also, the presentation here is not meant to be a comprehensive analysis of the control simulation but merely demonstrate that it is successful in achieving the primary goal of reproducing a steady state, category-1 hurricane that can be typically observed during the hurricane season of the western Atlantic and Caribbean Sea regions. A detailed investigation of the evolution and structure of the control simulation in reference to comparable observed hurricanes is deferred to a follow-up publication.

Figure 6 shows maximum 10 m wind speed (intensity hereafter) and minimum sea level pressure (MSLP) as a function of simulation time in the control simulation. Also shown are the intensity and MSLP time series from 76 perturbation simulations (see the next section for an explanation of how perturbation simulations were obtained). Generally speaking, the first 48 h of the simulations involve adjustment from the initial azimuthally averaged vortex to the environmental forcing as well as the development of the vortex-scale ocean structure underneath the simulated hurricane (not shown). It should be noted here that such adjustment

is due to not only the shortcomings of the initial vortex structure but also the imperfections of the numerical model such as numerical discretization, resolution, and physical parameterizations. It is, however, difficult and beyond the scope of the present study to quantify the contributions of these individual error sources. Instead, the focus is on the combined effect here, and this is interpreted as the “adjustment period.” In this period thus identified, both intensity and MSLP undergo noticeable fluctuations. After ~48 h into the simulations, it is evident that most simulations settle into a more steady regime where variations in intensity and MSLP are small in magnitude and occur on much shorter, $O(1 \text{ h})$, time scales. Although the intensity and MSLP envelope that encapsulates all perturbation simulations is relatively wide, most simulations are detected to closely follow this quasi steady state regime in the period of 48–96 h.

To demonstrate further the variability of intensity and intensification rate, frequency histograms are generated from their 48–96 h averages using each perturbation simulation as one sample. Here the typical operational definition of intensification rate is used; i.e., change in intensity in 24 h. According to Figure 7a, average 48–96 h intensity varies between 39 and 52 m s^{-1} , which corresponds to an intensity category range of 1–3. A sharp peak in frequency occurs at 46–47 m s^{-1} , which includes the control simulation. This category-2 intensity range is slightly greater than the original category-1 goal of the study, but within only 4–5 m s^{-1} of it. In terms of average intensification rate (Figure 7b), most simulations (with the exception of two outliers) vary between -4 and $+2 \text{ m s}^{-1} (24 \text{ h})^{-1}$, which is well within the steady state intensity range of -10 to $+10 \text{ kt} (24 \text{ h})^{-1}$ as defined earlier. The control simulation average intensification rate is $-1.5 \text{ m s}^{-1} (-2.9 \text{ kt})$, qualifying it as successful in terms of the goal of simulating a steady state hurricane.

Finally, the steady state vortex structure in the control simulation is briefly summarized in Figures 8 and 9. The evolution of the vortex

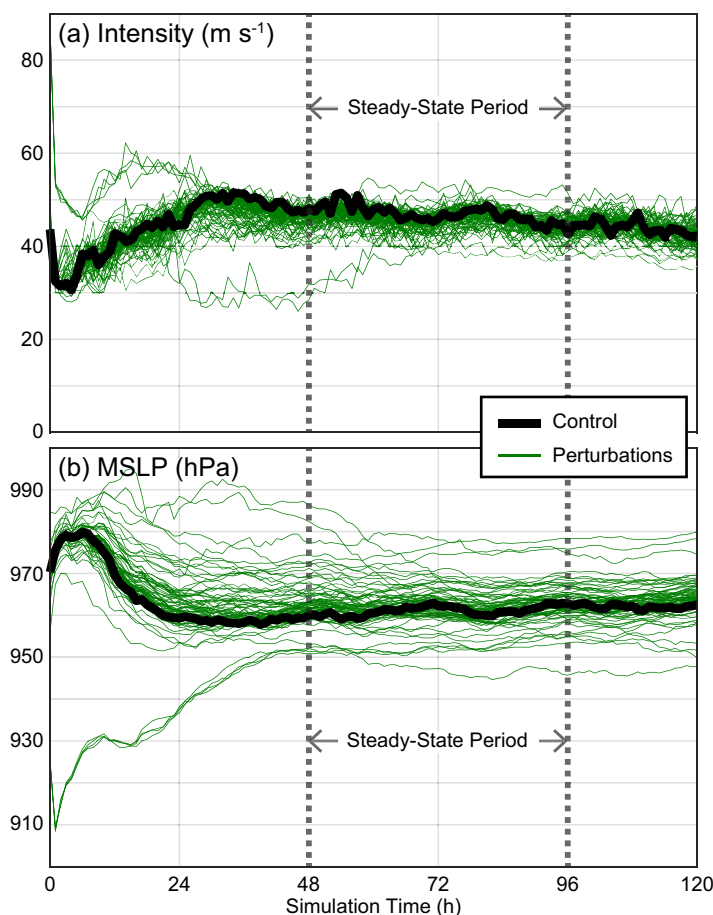


Figure 6. Time series of (a) intensity (m s^{-1}) and (b) MSLP (hPa) from the control (thick black lines) and perturbation simulations (thin green lines). The steady state period (48–96 h) is indicated with thick dotted lines.

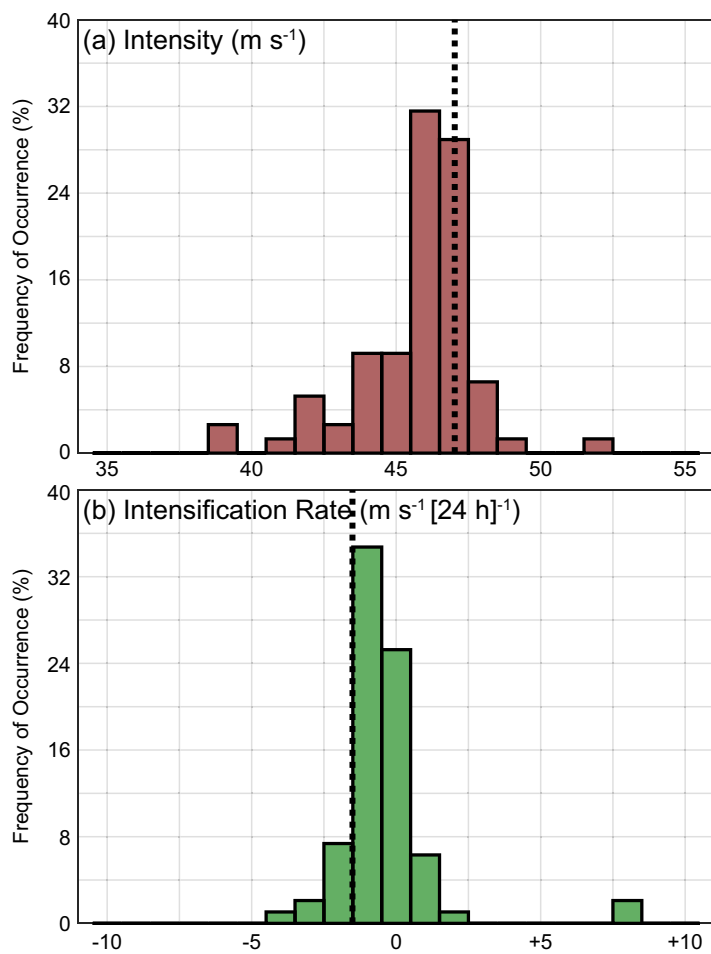


Figure 7. Frequency histograms (as percent of total number of simulations) of (a) intensity (m s^{-1}) and (b) intensification rate ($\text{m s}^{-1} [24 \text{ h}]^{-1}$). Quantities are averaged within the 48–96 h steady state window before frequencies are computed. Values from the control simulation are indicated with thick dotted lines.

azimuthally averaged kinematic and thermodynamic structures is illustrated in Figure 8. Fields at 0 h represent the direct outcome of the observation-based vortex initialization procedure explained in section 3 without any influence of model integration. All fields generally exhibit characteristics typically observed in category-1 hurricanes. The strongest azimuthal tangential wind is located within the inflow layer, regarded as the boundary layer jet in literature (Zhang et al., 2011). The secondary circulation is represented by the strongest inflow near the surface and outflow at upper levels (~ 12 km). Immediately above the inflow layer, an outflow jet feature is observed which is related to the supergradient flow according to boundary layer dynamics (Kepert, 2001). Above the boundary layer, a broad but weak ($< 6 \text{ m s}^{-1}$) radial outflow region exists between the heights of 8 and 16 km. This is one of the least realistic features of the observed vortex because it is traditionally one of the most severely subsampled regions in a hurricane vortex by reconnaissance aircraft (see section 3.2).

In terms of the thermodynamic structure, the peak of the warm-core intensity is ~ 7 K, analyzed in the observation-based vortex at a height of ~ 11 km. The peak moisture perturbation is located lower, mostly within the PBL (0–2 km height). While the warm-core structure is consistent with earlier studies in the literature (e.g., Durden, 2013; Stern & Nolan, 2012; Zhang & Chen, 2012), to the best knowledge of the authors, the low-level moisture anomaly is not studied in detail in the literature before.

The evolution of the vortex from the initial analysis to 72 h (center of the steady state period, see Figure 7) is depicted in Figures 8b and 8d. Kinematically, both the primary and secondary circulations appear to have strengthened at 72 h. This is consistent with the slight intensification of the vortex itself from category-1 hurricane intensity to category-2. Furthermore, a vertically deeper tangential wind speed structure is obtained along with much stronger and spatially better defined upper level outflow. As for the thermodynamic structure, the main difference is in the strengthening and lowering of the warm-core anomaly to ~ 11 K intensity and ~ 7 km height. A slight strengthening of the moisture perturbation is also apparent.

While the strengthening of the warm-core can be attributed to the slight overall intensification of the simulated vortex (e.g., Stern & Nolan, 2012; J. A. Zhang et al., 2015), the dependence of the warm-core anomaly height on intensity is still in debate (e.g., Durden, 2013; Stern & Nolan, 2012; Zhang & Chen, 2012). The reasons for the warm-core height evolution in the control simulation are beyond the scope of the present paper and remain to be explored in a future study. Above all, Figure 8 confirms that the observation-based initial vortex can be used to obtain a near-steady-state idealized hurricane simulation with realistic characteristics, with the obvious caveat that any departures in the simulated 72 h vortex state from the initial are due to various sources of model error such as, but not limited to, imperfections in physics parameterizations of surface and boundary layers, microphysical processes, and radiative transfer.

The 10 m wind speed (Figure 9a) represents a well defined, mostly symmetric eye and a mean RMW of ~ 69 km. Furthermore, the eyewall and rainband structures are well represented in the column precipitable water field (Figure 9b). Generally, larger values north of the center suggest a preferred region of convection to the left of the shear vector (due east, Figure 9a). As for the upper ocean structure, distinct SST and MLD perturbations in the wake of the hurricane relative to the storm motion vector (mostly to the northwest, Figure 9a) are the direct result of the atmosphere-ocean coupling in the simulation. Barring the limitations of the one-dimensional nature of the ocean model employed, the perturbations of SST (Figure 9c) and MLD (Figure 9d) appear reasonable and qualitatively compare well to previous studies (e.g., Ginis, 2002; Price, 1981).

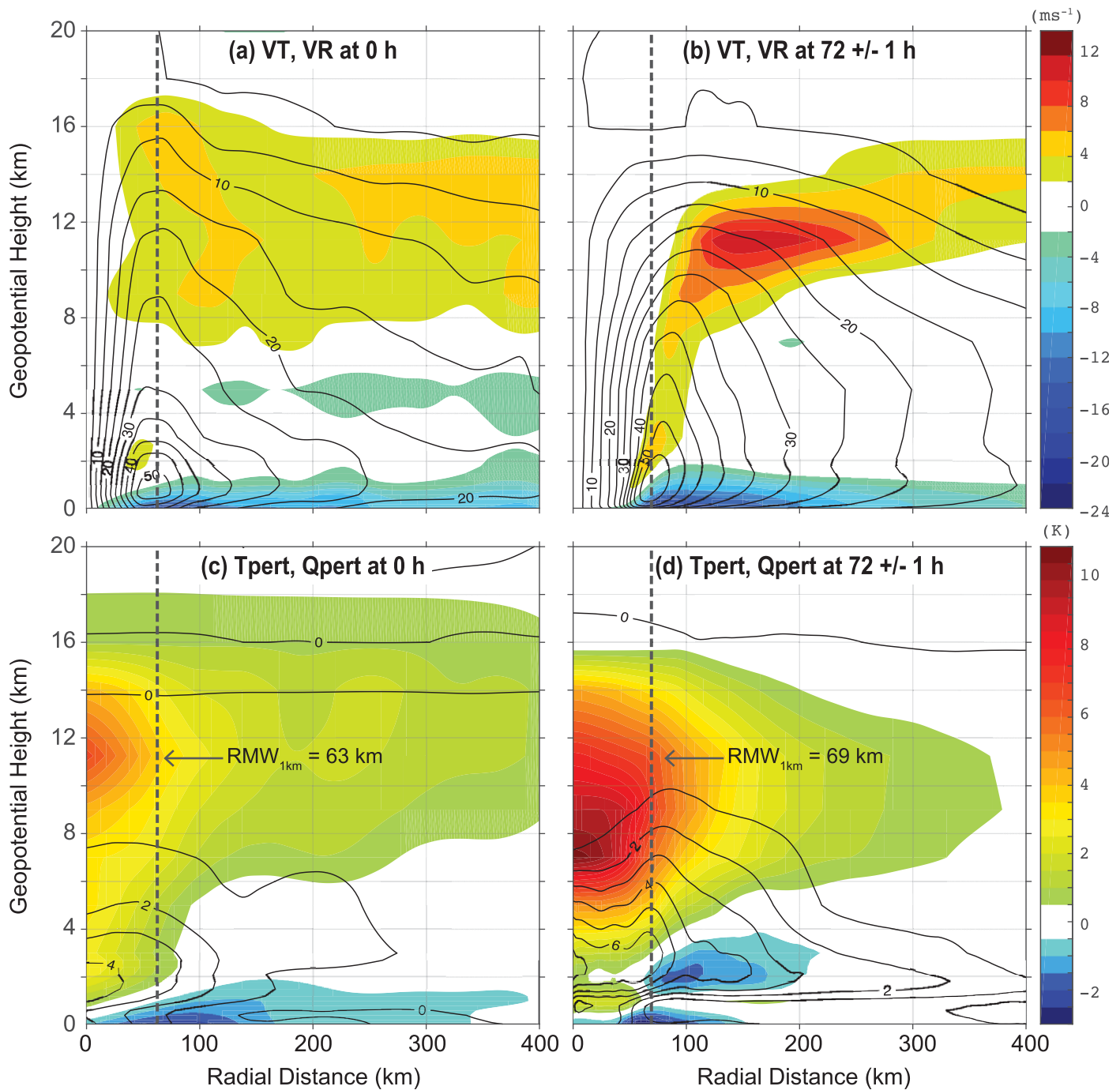


Figure 8. Radius-height cross sections of various azimuthally averaged fields at simulation times (left) 0 h and (right) 72 ± 1 h (mean). Plotted fields are (top) tangential wind speed (VT; shaded; m s^{-1}) and radial wind speed (VR; contoured; m s^{-1}) and (bottom) temperature perturbation (Tpert; shaded; K) and specific humidity perturbation (Qpert; contoured; g kg^{-1}). Radial distance is measured relative to respective storm centers. One kilometer radius of maximum wind ($\text{RMW}_{1\text{km}}$) is indicated with dashed lines. All perturbations are from azimuthal means at a distance of 500 km from respective storm centers.

5. Vortex-Scale Ocean Initialization: A Statistical Approach

In the present study, initialization of the ocean within the hurricane vortex is carried out using two different methods. In the first method, no vortex-scale ocean initialization is performed and the entire ocean structure is spun up from horizontally uniform profiles of temperature and salinity, as explained in section 2.3.2. This allows the ocean model to develop the vortex-scale ocean fields gradually, but consistent with the evolution of the atmospheric vortex. We deem the simulation thus obtained the “control” simulation.

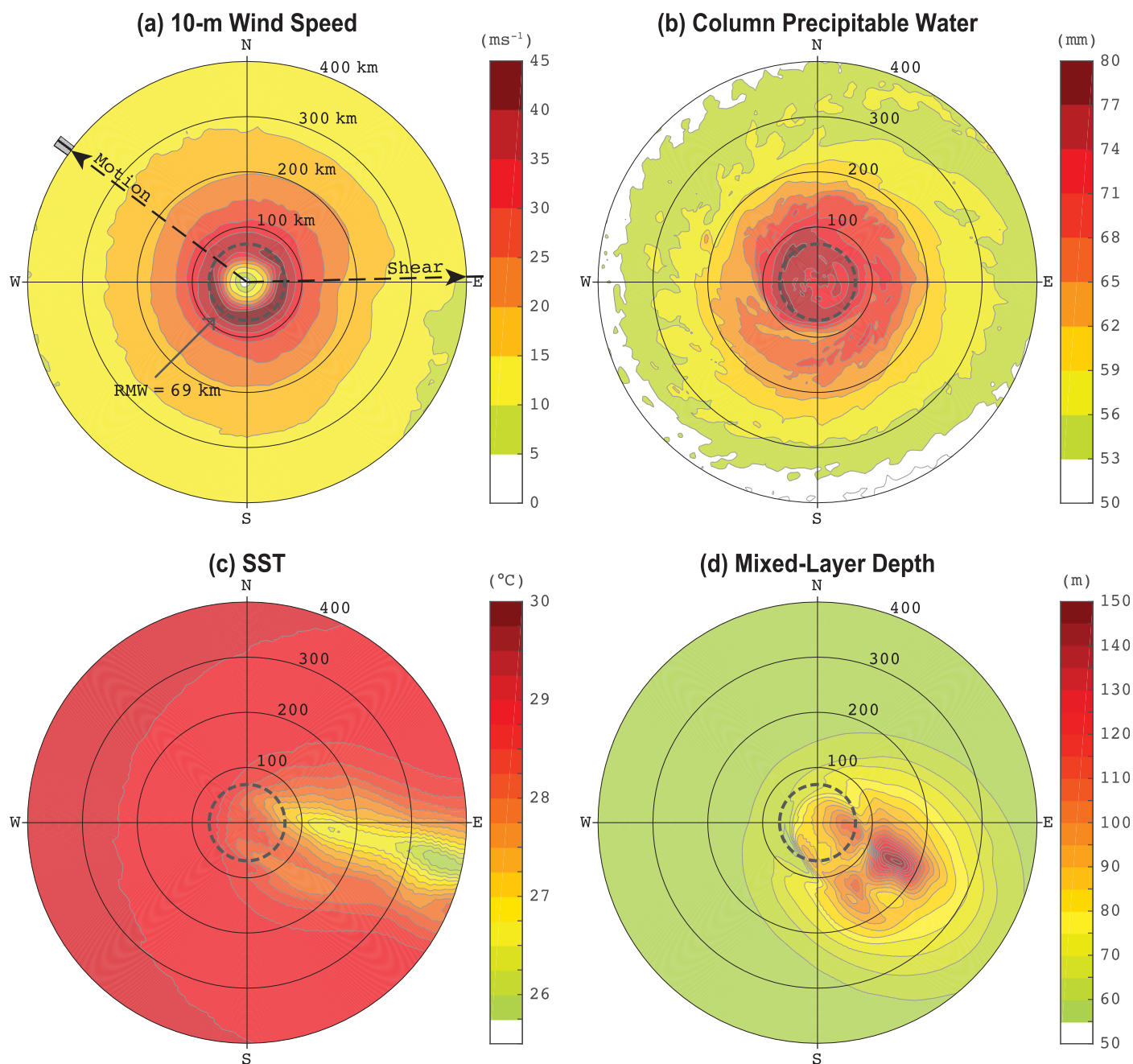


Figure 9. Plan view of storm-relative fields obtained from the steady state phase of the control simulation (averaged within 72 ± 1 h of simulation). Storm motion and shear directions are shown with dashed arrows (bands at the tip of arrows indicate range of values within averaging time window). RMW is shown by the dashed circle. Plotted fields are (a) 10 m wind speed (m s^{-1}), (b) column precipitable water (mm), (c) SST ($^{\circ}\text{C}$), and (d) ocean mixed-layer depth (m).

An alternative method for initializing the vortex-scale ocean temperature and salinity profiles that accounts for SST and MLD perturbations is also described. Here positive SST perturbation indicates SST cooling and positive MLD perturbation indicates mixed-layer deepening. This convention is consistent with the upper ocean perturbation structures commonly observed in hurricanes (Cione & Uhlhorn, 2003). Since oceanic observations within or near the hurricane inner core are not as common as their atmospheric counterparts, the composite observation-based technique described above for the atmospheric vortex initialization could not be attempted for the ocean. Therefore, a statistical approach is rather taken that attempts to exploit correlations between atmospheric and ocean fields. These correlations are calculated using several idealized

Table 3
Perturbations in the Configuration of the Idealized Model to Obtain the Various Simulations Used to Calculate Correlations Between Ocean and Atmospheric Fields for Vortex-Scale Ocean Initialization

	Control	Perturbation range ^a
Zonal vertical wind shear ^b (m s^{-1})	8	8
Westward storm speed ^c (m s^{-1})	5	5
Ambient SST ^c ($^{\circ}\text{C}$)	29	2
Ambient PBL (1,000–850 hPa) moisture (% RH ^d)	As in sounding	20
Ambient midlevel (850–500 hPa) moisture (% RH)	As in sounding	20
Ambient PBL (1,000–850 hPa) temperature (K)	As in sounding	2
Ambient midlevel (850–500 hPa) temperature (K)	As in sounding	2
Radius of maximum wind (km)	45	30
Initial intensity (kt)	85	20

^aFor each category, perturbations are always set to $\pm 100\%$, 50% , 25% , and 12.5% of the stated perturbation range, which amounts to eight simulations per category in addition to Control.

^bTwo additional perturbations include shear values of 20 and 24 m s^{-1} .

^cOne additional perturbation includes the combination of 0 m s^{-1} storm speed and ambient SST of 27°C .

^dRelative humidity.

“perturbation” simulations with the coupled model of the present study, during periods when simulated hurricanes remain in quasi steady state.

Table 3 lists the various perturbation simulations; no vortex-scale ocean initialization was employed in any of these perturbation simulations. “Perturbation” in this context refers to a change in a single model characteristic from its “control” configuration. Typically, storm environment characteristics (vertical wind shear, storm speed, ambient SST, and various aspects of ambient thermodynamic profiles) or initial vortex characteristics (RMW and intensity) are varied. For each parameter, eight simulations are carried out using perturbations of $\pm 100\%$, 50% , 25% , and 12.5% of the ranges indicated in Table 3. With the control, a total of 76 perturbation simulations are obtained, which include two additional simulations for vertical wind shear (20 and 24 m s^{-1}) and one additional simulation with simultaneous storm speed (0 m s^{-1}) and SST (27°C) perturbations. How various model fields respond to these perturbations is not the focus of the present study and will be evaluated in detail in a separate publication in the near future. Nevertheless, a brief overview of the responsiveness of model simulations to parameter perturbations is provided in the subsequent section.

In each simulation, time series of several scalar vortex metrics are calculated. These metrics are chosen to represent various kinematic and thermodynamic aspects of the simulated hurricanes, but limited to those that can be calculated from the azimuthally averaged fields of the initial vortex so that ocean perturbation fields can be directly correlated to features of the initial observed vortex. Table 4 lists the 30 scalar metrics used in the present study. Metrics are grouped into four main categories that best indicate the specific vortex characteristic they represent. Care is given to achieve a broad representation of kinematic and thermodynamic properties of an axisymmetric hurricane vortex. Metrics related to cloud and hydrometeor composition are not considered, as they are not available in the initial observation-based vortex methodology described above.

For the ocean, azimuthally averaged SST and MLD perturbations are calculated at a relative radial spacing of 1 RMW between storm center and 5 RMW. This radial range is generally found to be sufficient to represent the maximum storm-relative SST and MLD perturbations in the simulations (also see Halliwell et al., 2015).

In the correlation analyses, hourly time series between simulation times of 2.5 and 3.5 days are used; this corresponds to a period when atmospheric and oceanic spin-up processes are complete and the simulated hurricanes are generally found to be in quasi steady state. To filter out transient features, moving-average filtering with a ± 3 h window is applied to all time series. With 24 time series data points in 76 simulations, a sample size of 1,824 is achieved for correlation calculations. Please see the supporting information (Supporting Information S1 and Data set S1) for data used in correlation and regression analysis calculations.

5.1. Model Response to Parameter Perturbations

A brief overview of model sensitivity to perturbed parameters is presented first to demonstrate the robustness of the perturbation methodology employed to obtain atmosphere-ocean correlation relationships. To

Table 4
Scalar Metrics Utilized in Correlation Calculations, as Related to Azimuthally Averaged Kinematic and Thermodynamic Vortex Characteristics

Metric	Description
1. Environment (Env)	
Speed (m s ⁻¹)	Storm speed
Shear (m s ⁻¹)	Vertical wind shear
SSTenv (°C)	Ambient ^a (Amb.) SST
Tenv900 (K)	Amb. temperature at 900 hPa
Qenv900 (g kg ⁻¹)	Amb. spec. humidity at 900 hPa
RHenv900 (%)	Amb. rel. humidity at 900 hPa
Tenv700 (K)	Amb. temperature at 700 hPa
Qenv700 (g kg ⁻¹)	Amb. spec. humidity at 700 hPa
RHenv700 (%)	Amb. rel. humidity at 700 hPa
2. Intensity (Int)	
MSLP (hPa)	Min. sea level pressure
Int (m s ⁻¹)	Max. 10 m wind speed (wspd)
VTmax (m s ⁻¹)	Max. tangential wspd (VT)
VRinmax (m s ⁻¹)	Max. radial wspd (VR) – inflow ^b
InfAng_RMw (°)	Inflow angle ^c at RMW
Vortmax (s ⁻¹)	Max. vorticity
VRoutmax (m s ⁻¹)	Max. VR – outflow ^b
Divmax (s ⁻¹)	Max. divergence
WCoremax (K)	Max. warm-core anom. ^d
3. Horizontal vortex structure (VortH)	
RMW (km)	Radius (rad.) of max. wind
R_VRinmax (km)	Rad. of max. VR inflow
R_InfAngmin (km)	Rad. of min. inflow angle
R_Vortmax (km)	Rad. of max. vorticity
R_Divmax (km)	Rad. of max. divergence
4. Vertical vortex structure (VortV)	
H_VTmax (m)	Height (hgt) of max. VT
H_VRinmax (m)	Hgt of max. VR inflow
H_PBLVR_RMw (m)	PBL hgt at RMW – for inflow ^e
H_PBLTv_RMw (m)	PBL hgt at RMW – for θ_v^f
H_Vortmax (m)	Hgt of max. vorticity
H_Divmax (m)	Hgt of max. divergence
H_VRoutmax (m)	Hgt of max. VR outflow
H_WCoremax (m)	Hgt of max. warm-core anom.

Note. Metrics are grouped in four categories according to the vortex feature they best represent.
^aAll ambient quantities are azimuthally averaged at a distance of 20° from storm center.
^bPositive radial inflow is radial wind toward the storm center; positive radial outflow is radial wind away from the center.
^cSee definition in Zhang and Uhlhorn (2012).
^dWarm-core anomaly is calculated at each vertical level as the temperature perturbation from azimuthal average at a distance of 10 RMW from storm center.
^eFollowing the definition of depth of the inflow layer in Zhang et al. (2011).
^fFollowing the definition of mixed-layer depth in Zhang et al. (2011), using equivalent potential temperature (θ_v).

measure cumulative atmospheric sensitivity to the parameter perturbations described in Table 3, a model-based version of the response function introduced by Tong and Xue (2008; their equation (6)) is derived as follows:

$$J_{p,r}^M = \frac{1}{\sigma_{ctr}^M} \left[\frac{1}{N_t} \sum_{t=1}^{N_t} (M_{p,r}^t - M_{ctr}^t)^2 \right] \quad (9)$$

Here J denotes the response function and measures the normalized squared distance of a given model metric (M) time series from the corresponding control-run (subscript “ctr”) time series. Time series are calculated for hourly simulation time window $t = 2-4$ days ($N_t = 48$). Normalization is carried out using the standard deviation of the control-run time series, σ_{ctr}^M . Response function calculation is repeated for all of the perturbation parameters p and their realized values r in Table 3, as well as for all of the vortex-related scalar metrics M in Table 4 (groups 2–4). Finally, for each parameter and its realizations, cumulative response functions are calculated by averaging all metric-based response functions:

$$J_{p,r} = \frac{1}{N_M} \sum_{M=1}^{N_M} J_{p,r}^M \quad (10)$$

where $N_M = 22$ is the number of scalar metrics considered in the calculation.

Figure 10 illustrates how $J_{p,r}$ varies in the present study. In general, simulated vortex characteristics appear to be sensitive to parameter perturbations in varying degrees. In the small parameter perturbation range (within ± 0.5 in terms of normalized parameter perturbation values), model sensitivity to environmental parameters is mostly comparable. Meanwhile, perturbations in intensity and RMW lead to quicker responses, which then flatten out at larger perturbation realizations. Not surprisingly, the spread among parameters in the amount of model response increases at higher perturbation values ($>|0.5|$). In this range, parameters RMW, Shear, and SSTenv lead to the strongest overall vortex sensitivity and SSpeed to the smallest. Nevertheless, parameter sensitivity appears to be generally comparable for most parameters, especially considering that Figure 10 represents the cumulative response of 22 vortex-related metrics. Overall, selection of parameters and their range of perturbations appear suitable for a robust correlation analysis.

5.2. Correlation Analysis

Based on the samples as described above, Pearson correlation coefficients (henceforth referred to as “correlations”) are calculated for the atmospheric vortex metrics and SST/MLD perturbations. These correlations are summarized in Figure 11. In the atmosphere, a natural separation is apparent between metrics that represent the environment

(group Env) versus the vortex (groups Int, VortH, and VortV), where strong cross correlations exist within-group rather than across-group. The exception here seems to be height of maximum radial outflow (H_VRoutmax), which is more strongly correlated with environment metrics than vortex metrics. Within the vortex-related metrics themselves, further separation can be inferred for intensity (group Int) versus vortex structure (groups VortH and VortV), although distinctions are not as clear-cut. One obvious variable is maximum vorticity (Vortmax), which, although listed within the group Int, is most strongly correlated with RMW and radius of maximum radial inflow (R_VRinmax) in the VortH group. This correlation is presumably due to

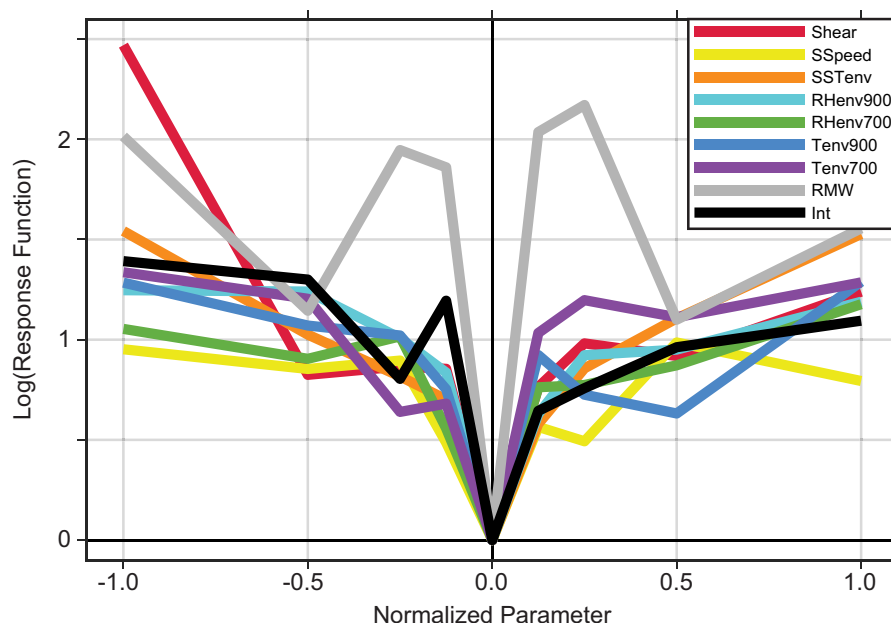


Figure 10. Cumulative response function for perturbation parameters and their various realized values. Each perturbed parameter is represented by a different color. Parameter realizations are normalized by their respective maximum deviation from the control, so that -1 , 0 , and 1 on the x axis represent the minimum, control, and maximum realization values, respectively. Response functions are plotted on the log scale for easier visualization.

the fact that vorticity is related to the radial gradient of the horizontal wind, which is strongly influenced by the horizontal size of the vortex.

It should be noted here that Figure 11 also summarizes the sample means and standard deviations for all vortex metrics and SST/MLD perturbations. A quick glance at the vortex metric means suggests that on average, the idealized simulations produced a hurricane vortex with most characteristics that are consistent with those observed typically in steady state, strong category-1 hurricanes. Mean intensity is 46 m s^{-1} , which is accompanied by a mean MSLP of 962 hPa and a mean RMW of 68 km. The mean RMW is somewhat larger than typically observed (40–50 km; e.g., Hsu & Yan, 1998) and reflects the general trend of increasing vortex size during the simulations. Vertically, the mean PBL depth at RMW is $\sim 1.3 \text{ km}$ kinematically (based on radial inflow speed, H_{PBL} , VR_{RMW}) and $\sim 310 \text{ m}$ thermodynamically (based on equivalent potential temperature, θ_v , H_{PBL} , Tv_{RMW}), both of which are slightly greater than observed as reported by Zhang et al. (2011). Above the PBL, a mean warm-core anomaly (WCoremax) of magnitude 11 K is encountered at the height (H_{Wcoremax}) of 7.4 km, which is consistent with previous numerical studies (e.g., Stern & Nolan, 2012). In the ocean, sample means of both SST and MLD perturbations are maximized in the radial range of 0–1 RMW at values of 0.63°C and 24 m. For SST, although maximum cooling appears to occur at a smaller magnitude and much closer to the storm center than in Halliwell et al. (2015; see discussion in their section 4.c), we note that here, all calculations are performed in an azimuthally averaged sense. Since SST cooling typically occurs in a narrow region in the right rear quadrant and thus attains an increasingly higher wave number structure with increasing radial distance (see Lorsolo & Aksoy, 2012, for a discussion on azimuthal wave number decomposition in a hurricane vortex), its amplitude cannot get projected effectively onto wave number 0 at the distances of 3–5 RMW where it is maximized.

Meanwhile, in terms of sample variability, expressed here as sample standard deviation normalized by sample mean, greater spread is observed for vortex structure and intensity than storm environment, with the exception of vertical shear and storm speed that are varied in a greater range in perturbation simulations than the other environment perturbations (see Table 4). It is interesting to note that, although intensity and MSLP show very small spread, presumably because simulated hurricanes are in quasi steady state, strong variability is nevertheless observed in the vortex structure. This suggests the possibility of a sufficiently strong relationship between the vortex and ocean structures to construct a regression model with statistical significance.

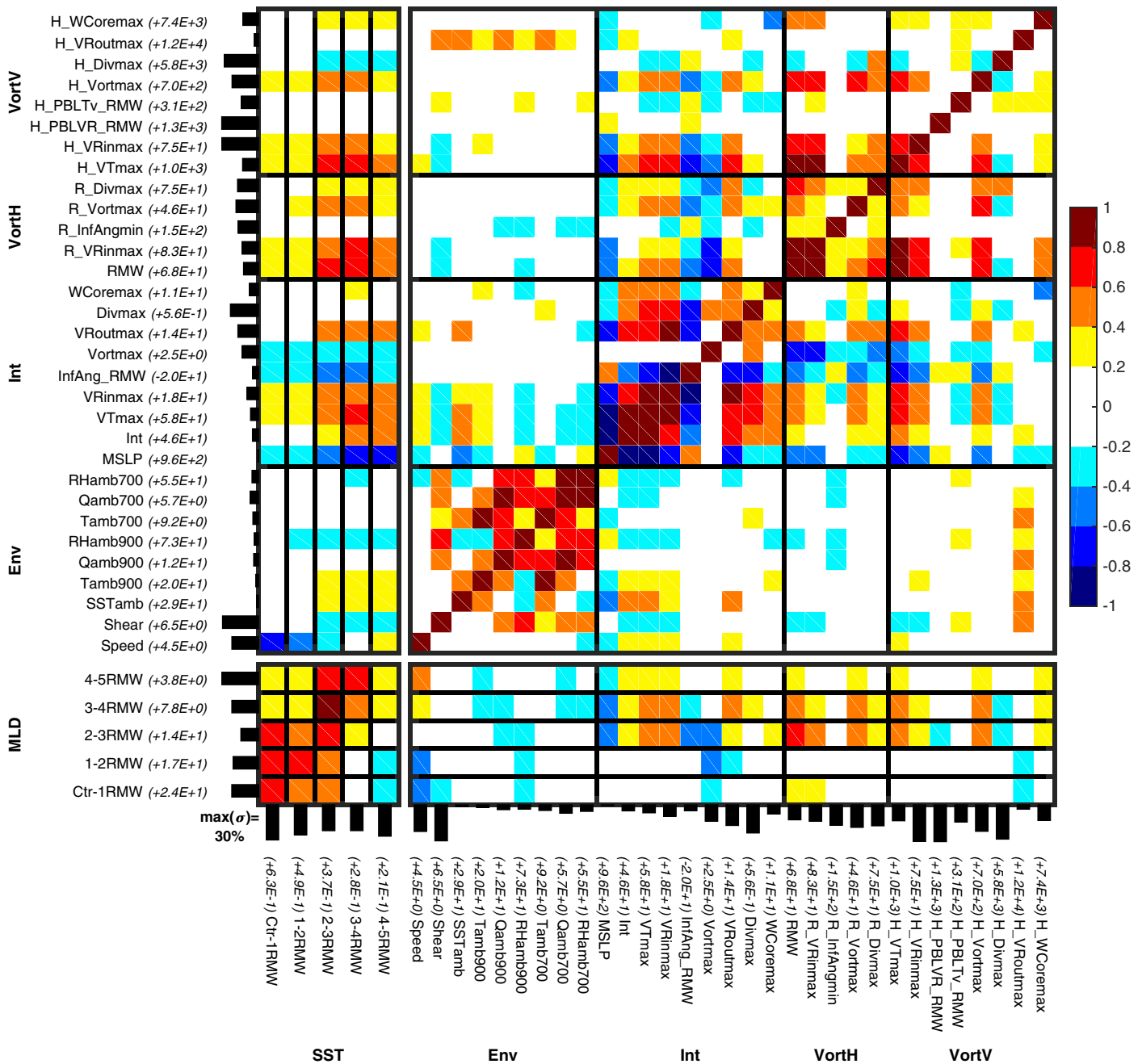


Figure 11. Pearson correlation coefficients for atmospheric vortex metrics and SST/MLD perturbations. (top right) Correlations among atmospheric variables. (bottom left) Correlations between SST and MLD perturbations within 0–5 RMW. (top left) Correlations between atmospheric variables and SST perturbations. (bottom right) Correlations between atmospheric variables and MLD perturbations. Mean values for individual variables are indicated in parentheses in italic next to their labels. Standard deviations are indicated as black bars next to respective variables (measured as percent of mean and normalized by the maximum value of 30%).

Moving on to atmospheric correlations, a rich cross-dependence among variable groups as well as individual variables is indicated in Figure 11, suggesting that further reduction of dimensionality would require a more complex analysis of orthogonality to obtain a robust regression relationship with the smallest possible number of independent variables. On the ocean side, a noticeable separation exists in the ocean-atmosphere cross correlations between the radial ranges of 0–2 RMW and 2–5 RMW, especially for SST perturbations. In the 0–2 RMW range, stronger correlations are found with the environment variables, and especially storm speed. Clearly, and perhaps not surprisingly, in the inner core of hurricanes, the strongest

contributor to SST cooling is storm speed: a negative correlation means that slower storms experience greater SST cooling in the inner core, which is consistent with previous observational and modeling studies (e.g., Cione & Uhlhorn, 2003; Halliwell et al., 2015).

Beyond 2 RMW, the impact of storm speed on ocean perturbations decreases as correlations with vortex-specific metrics become more prominent. This implies that vortex intensity and structure are also important in determining the axisymmetric component of ocean perturbations in hurricanes, but only in regions outside the immediate inner core.

5.3. Reduction in Dimensionality: Principal Component Analysis Versus Factor Analysis

Although Figure 11 reveals a rich correlation structure among environment, vortex, and ocean perturbation characteristics, reduction in dimensionality is still desired to obtain a robust regression model to estimate the initial ocean perturbation structure. Two alternative approaches are employed for this purpose: principal component analysis (PCA) and factor analysis (FA), which are two exploratory techniques used to identify

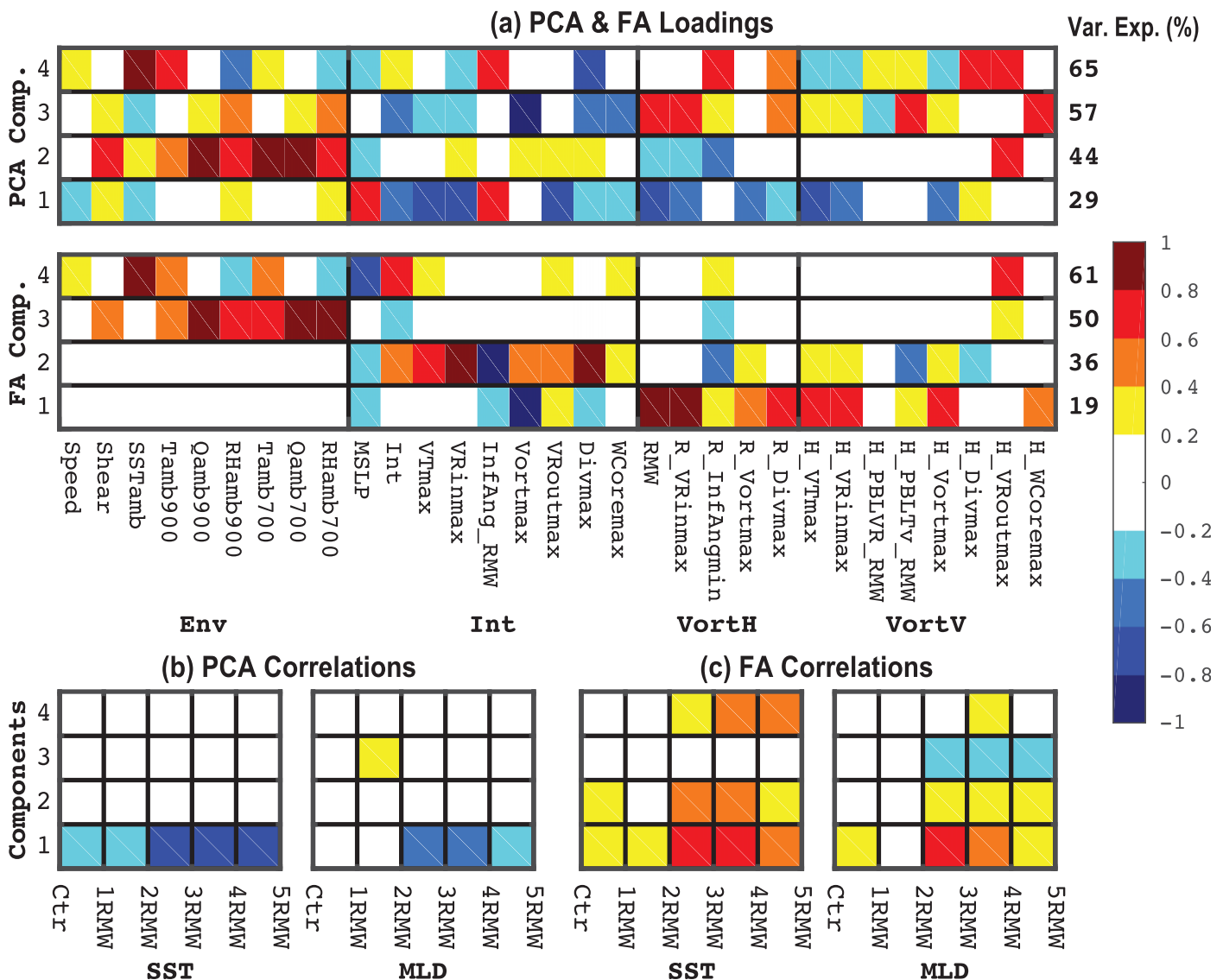


Figure 12. Summary of principal component analysis (PCA) and factor analysis (FA) results for the first four components. (a) Factor loadings by the atmospheric metrics. Cumulative variance explained (%) is indicated to the right of respective components. (b) Correlations between PCA components and ocean perturbations ((left) correlations with SST and (right) correlations with MLD). (c) As in Figure 12b but for FA components. Factor loadings in Figure 12a are normalized (separately for each component) by the maximum absolute loading value in each component.

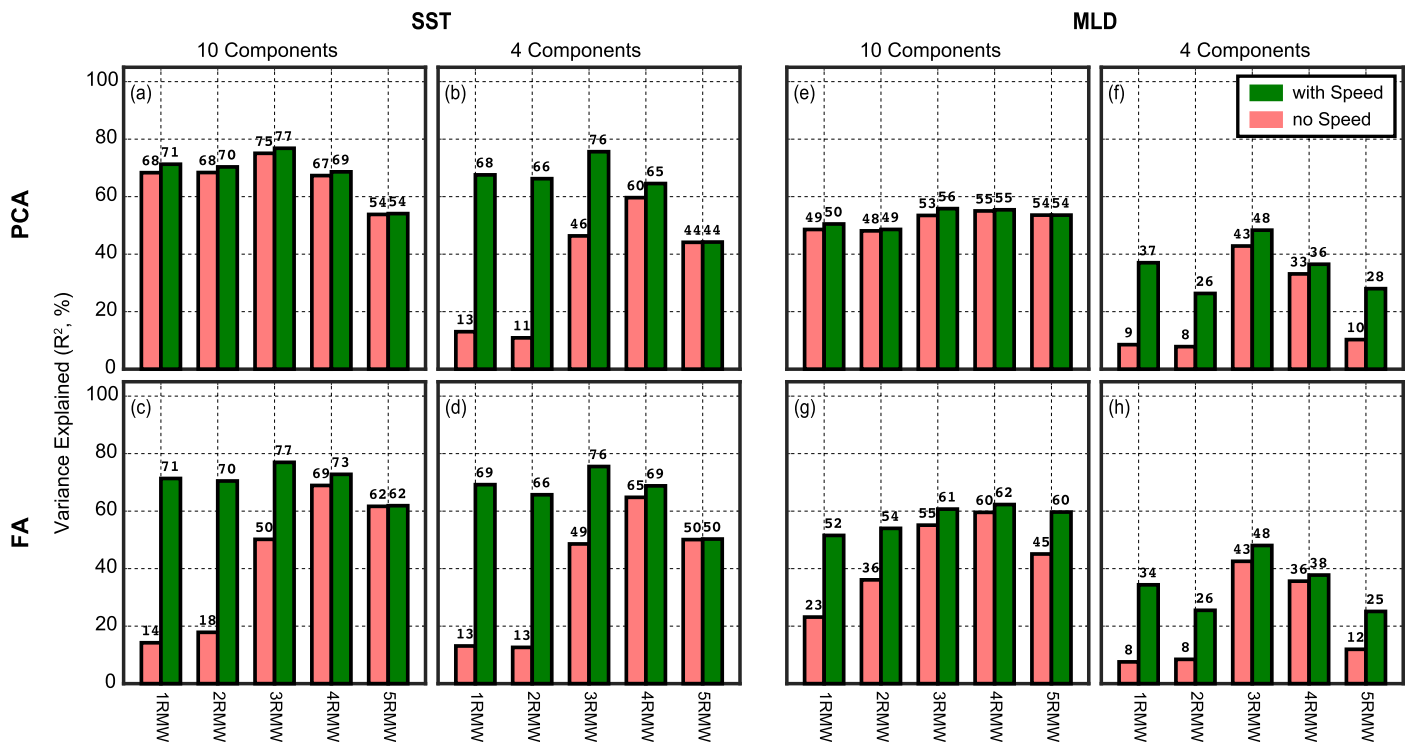


Figure 13. Summary of regression analysis results for SST and MLD perturbations. Each bar shows the variance explained (%) by one regression model (values also indicated above bars for ease of reference). (top row) Results using PCA components as independent variables. (bottom row) Results using FA components as independent variables. Green bars include storm speed as an additional independent variable while red bars indicate results using only respective PCA/FA components. Regression analyses are carried out in radial ranges between 0 and 5 RMW. For each ocean variable, results using 10 components are summarized on left panels while 4 components are shown in right figures.

coherent subsets in complex data sets (see e.g., Tabachnick & Fidell, 2001, for the technical details of these techniques). Variables are aggregated into components/factors according to their correlations, such that variables grouped within a component/factor are correlated with one another but mostly independent of other subsets of variables. These techniques are expected to be useful in the context of the present study to reduce the large number of atmospheric variables investigated into a smaller group that represents the common physical properties of the underlying variables. It should be noted that the most important difference between PCA and FA is that PCA analyzes variance, whereas FA analyzes covariance. As Tabachnick and Fidell (2001) describe: "The goal of PCA is to extract maximum variance from a data set with a few orthogonal components. The goal of FA is to reproduce the correlation matrix with a few orthogonal factors." A loading in this context refers to the normalized contribution by a variable to a specific component/factor.

Another important aspect of FA is in its utilization of rotational techniques, which generate mathematically equivalent solutions but are expected to expand the interpretability and scientific value of a solution

Table 5
Summary of the SST-Perturbation Regression Model Statistics

	Contributing metrics	Estimate (°C)	Std. err. (°C)	t stat.	p value
Intercept		1.302	0.0119	109.5	0
SSpeed		-0.149	0.0026	-57.6	0
Comp. 1	RMW, R_VRinmax, H_VTmax, Vortmax	0.071	0.0023	30.5	2.5E-165
Comp. 2	VRinmax, InfAng_RMW, Divmax, VTmax	0.052	0.0023	22.0	1.8E-95
Comp. 3	Qamb700, RHamb700, Qamb900, Tamb700	-0.024	0.0024	-10.0	7.6E-23
Comp. 4	SSTamb, Int, MSLP, H_VRoutmax	0.050	0.0023	21.4	6.3E-91

Note. First four contributing metrics with highest absolute loading for each component are also shown.

Table 6
Summary of the MLD-Perturbation Regression Model Statistics

Contributing metrics		Estimate (m)	Std. err. (m)	t stat.	p value
Intercept		37.788	0.4333	87.2	0
SSpeed		-3.070	0.0941	-32.6	5.4E-184
Comp. 1	R_VRinmax, RMW, H_VTmax, H_Vrinmax	1.345	0.0847	15.9	3.2E-53
Comp. 2	InfAng_RMW, Divmax, VRinmax, VTmax	0.234	0.0831	2.8	4.9E-3
Comp. 3	Int, MSLP, SSTamb, H_VRoutmax	0.302	0.0879	3.4	6.1E-4
Comp. 4	RHamb900, Qamb900, Shear, Qamb700	-1.977	0.0855	-23.1	7.7E-104
Comp. 5	Tamb900, Tamb700, Qamb900, Qamb700	0.529	0.0844	6.3	4.6E-10
Comp. 6	H_Wcoremax, WCoremax, VRoutmax, H_PBLTv_RMW	-0.050	0.0784	-0.6	5.2E-1
Comp. 7	H_Divmax, R_Divmax, R_Vortmax, H_PBLTv_RMW	-0.227	0.0848	-2.7	7.5E-3
Comp. 8	R_InfAngmin, R_Vortmax, H_VRinmax, Vortmax	-0.107	0.0814	-1.3	1.9E-1
Comp. 9	SSTamb, H_PBLTv_RMW, MSLP, H_Wcoremax	-1.193	0.0780	-15.2	9.1E-50
Comp. 10	RHamb700, Qamb700, RHamb900, Tamb900	0.615	0.0837	7.3	3.2E-15

Note. First four contributing metrics with highest absolute loading for each component are also shown.

(Tabachnick & Fidell, 2001). Various orthogonal rotational techniques typically used in practice, such as varimax, quartimax, and equamax, are explored in the present study but were observed to produce qualitatively similar distributions of factor loading (not shown). Therefore, results are shown only using the varimax technique, which is the most commonly used rotation available.

Figure 12 explores factor loadings by the atmospheric metrics for the first four PCA and FA components, as well as the cross-correlation structures of these components with SST and MLD perturbations. Four is chosen for the number of components for the purpose of easier visualization and because it matches the number of variable groups. From Figure 12a, in both PCA and FA, the first four components explain ~60–65% of total variance (increasing to ~85% with 10 components, not shown), with lower ranked components explaining more variance than higher-ranked ones by design. Loadings in Figure 12a indicate each variable's normalized representation in a particular component of PCA or FA.

Both techniques give more prominence to intensity and vortex structure than environment as the larger loadings of the first two components mostly coincide with these groups. However, in general, FA components seem to be more strongly correlated with distinct variable groups (i.e., more distinct partitioning of loadings into unique variable groups in FA). This suggests that FA provides a dimension reduction that is more physically intuitive in nature, because variable groups represent various unique aspects of our physical understanding of hurricane vortex dynamics.

Focusing further on the FA components in Figure 12a, from the loadings of the first component it appears that vortex structure (both horizontal and vertical) is the strongest contributor to the overall atmospheric correlation matrix. An exception is vorticity (its maximum magnitude as well as height and radius of its maximum magnitude), which is originally categorized as an intensity variable but appears more strongly associated with structure. In other words, statistically speaking, vorticity is more strongly influenced by the size of a vortex than the strength of its circulation, a finding that is consistent with the preceding correlation analysis. The second and third FA components are distinctly correlated with intensity and environment, respectively. The fourth component is also interesting, in the sense that it links variables from three variable groups: ocean-surface and atmospheric temperature (group Env), intensity, MSLP, and maximum radial outflow (group Int), and height of maximum radial outflow (group VortV).

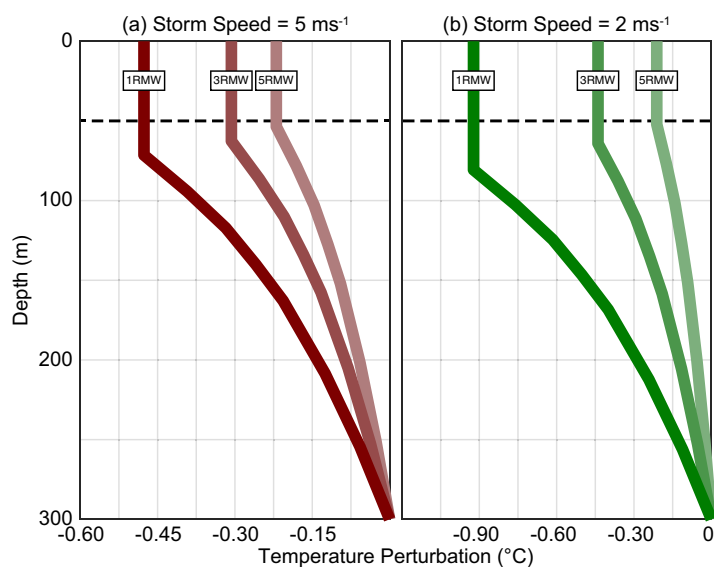


Figure 14. Ocean temperature perturbation structures obtained with the regression models that utilize 4 FA components (SST) and 10 FA components (MLD) as well as storm speed as independent variables. The perturbed SST is applied to the depth of the perturbed mixed layer (nonperturbed MLD indicated by the dashed lines). Perturbations are then linearly damped until zero perturbation is reached at the depth of 300 m. Temperature perturbations are shown for two storm speed values: (a) 5 m s^{-1} and (b) 2 m s^{-1} .

Finally, in Figures 12b and 12c, correlations between the PCA and FA components and SST and MLD perturbations are summarized. In both techniques, correlations are generally strongest for the first component and for radii outside 2 RMW. This outcome is consistent with the previous finding of strong relationship between intensity and vortex structure groups and ocean perturbations in the same radial range of 2–5 RMW (Figure 11). Ocean perturbations are, however, only weakly correlated with the PCA and FA components in the inner core, where they were previously found to be strongly correlated with storm speed (Figure 11). This suggests that it may be necessary to consider storm speed as a separate independent variable in the regression analysis, in addition to the PCA or FA components.

5.4. Regression Model for Ocean Perturbations

The final step in the estimation of the initial radial structure of ocean perturbations is to construct a linear regression model based on the findings of the preceding correlation and PCA/FA analyses. For this purpose, mean SST and MLD perturbations within increments of 1 RMW between 0–5 RMW are estimated independently, using either PCA or FA components. Since an additional 20% atmospheric variance is explained with 10 components versus four, to ensure robustness, separate regression analyses are carried out with four and 10 components as independent variables. A further set of regression analyses is also performed with storm speed as an additional independent variable. All results are summarized in Figure 13.

For SST perturbations, using 10 components as independent variables from either the FA or PCA analysis adds only marginally to the variance explained (R^2) of the regression models obtained at various radial ranges, compared to using four components. Meanwhile, using storm speed as an additional independent variable generally contributes positively to R^2 , especially within 0–3 RMW, except when using 10 PCA components because storm speed provides a strong loading on the ninth PCA component already (not shown). Overall, R^2 values of ~70% or slightly above are achieved within 0–4 RMW with the addition of storm speed as an independent variable.

For MLD perturbations, regression models are less robust overall, reaching only ~60% R^2 at the most. There is also greater benefit from using 10 components versus four in both PCA and FA, further indicating that it is more difficult to estimate MLD structure from atmospheric variables than SST. This outcome is in line with preceding findings from correlation analysis and PCA/FA. Impact of storm speed on R^2 is similar to that in SST, with significant contributions within 0–3 RMW except in the case of 10 PCA components as before.

The coefficients of one regression model each for SST and MLD perturbations are given here that are believed to result in the most robust estimations with most physical consistency and least possible complexity. For SST, the four-component FA regression model with storm speed as an additional independent variable is able to provide a sufficiently robust variance explained (see Table 5 for summary). For MLD, the generally weaker correlation signals necessitate inclusion of up to 10 components in the FA model (with storm speed) to achieve the highest possible variance explained (see Table 6 for summary). Because MLD coefficient estimates for FA components 6 and 8 are not statistically significant (i.e., p values do not meet the 95% confidence criterion), these two components are omitted in the final regression model with an almost identical overall R^2 score (not shown).

Using the regression models described above for SST and MLD perturbations, an azimuthally averaged initial ocean perturbation structure is obtained that corresponds to desired initial atmospheric characteristics and storm speed. These perturbation profiles are then added to

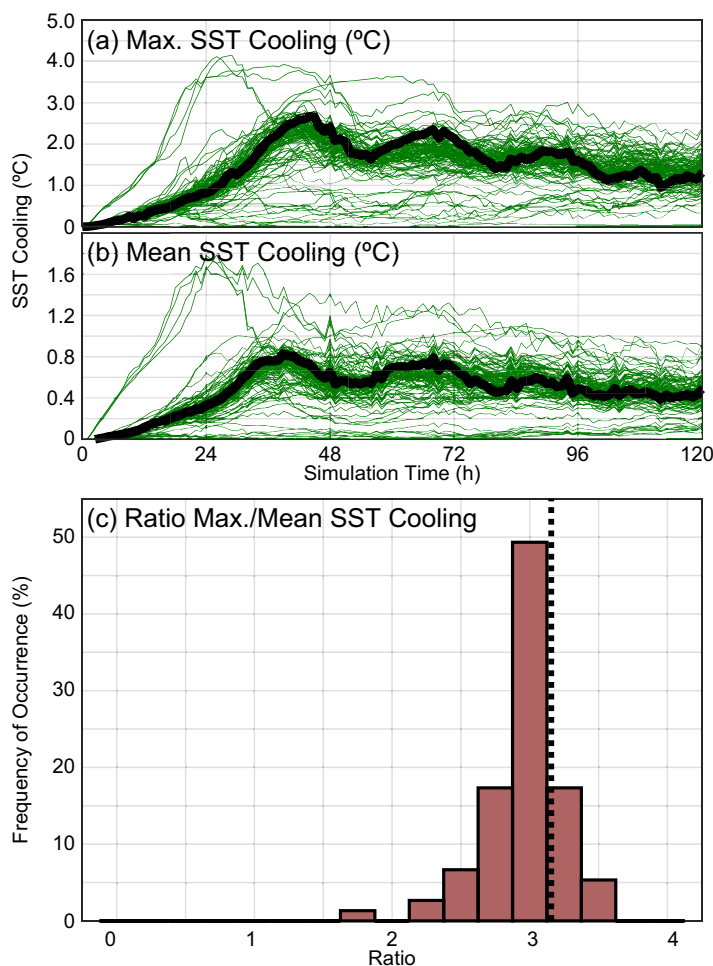


Figure 15. Time series of (a) maximum SST cooling (°C) and (b) azimuthally averaged SST cooling (°C) from the control (thick black line) and perturbation simulations (thin green lines). Quantities are calculated within 0–100 km of the storm center. Frequency histogram (as percent of total number of simulations) of the ratio of maximum-to-mean SST cooling is shown in (c). Quantities are averaged within the 48–96 h steady state window before frequencies are computed. Value from the control simulation is indicated with a thick dotted line.

the climatological profile (Figure 3) to obtain full temperature perturbation profiles. Corresponding salinity profiles are generated by compressing the 50–300 m climatological profile to a shorter depth due to increased MLD, maintaining the climatological magnitudes (not shown). Figure 14 provides two such temperature profiles for the initial atmospheric characteristics of the control simulation and storm speeds of 5 and 2 m s⁻¹, calculated at varying radial ranges. For the storm speed of 5 m s⁻¹, which is used in the control simulation, a peak azimuthally averaged SST cooling of ~0.5°C is obtained within 1 RMW of the storm center, along with an MLD perturbation of ~20 m. At the range of 4–5 RMW, the perturbation drops to ~0.2°C. The strong inner-core dependence on storm speed is clearly demonstrated in this regression model at the slower speed of 2 m s⁻¹ with almost doubled SST cooling of ~0.9°C and MLD perturbation of ~30 m within 1 RMW from storm center. However, such dependence is almost nonexistent at 4–5 RMW as perturbations remain mostly unchanged from 5 m s⁻¹.

6. Summary and Discussion

A new vortex-scale initialization scheme is presented for idealized coupled hurricane simulations. The atmospheric scheme involves construction of azimuthally averaged kinematic and thermodynamic initial fields based on historical composite data sets from hurricane reconnaissance aircraft. The main data sources for these composites are the dropsonde database of Zhang and Uhlhorn (2012) and a large database of airborne Doppler-radar-derived three-dimensional wind fields in hurricanes (e.g., Rogers et al., 2013b). For ocean initialization, observations of the upper ocean within hurricanes are much less common than their atmospheric counterparts. Therefore, a statistical scheme is proposed that takes advantage of the many perturbation simulations carried out with the present idealized hurricane model to construct a regression model for the azimuthally averaged ocean (SST and MLD) perturbation fields in the vortex.

While the main goal of the present study is not to investigate in detail the vortex structure of the idealized coupled simulations, a brief overview of intensity and intensification rate in the control simulation and perturbation simulations nevertheless indicates that almost all of the simulations remain approximately steady with a narrow frequency distribution for intensity between 39 and 52 m s⁻¹ that has a mode of 46–47 m s⁻¹. This mode corresponds to category-2 intensity that is slightly greater than the category-1 target of the simulations, but within only 4–5 m s⁻¹ (~10%) of it. Overall, it is concluded that the simulations are successful in producing steady state hurricanes of near-category-1 intensity.

The statistical ocean initialization scheme requires a large number of samples of atmospheric and ocean fields so that robust regression relationships can be obtained. To achieve this, perturbation simulations are carried out centered on the control simulation, only changing a single parameter of storm environment or initial vortex at a time. For each such parameter, eight simulations are carried out with the exception of two additional simulations for vertical wind shear and one additional simulation with simultaneous storm speed and SST perturbations. With the control, a total of 76 perturbation simulations are thus obtained. A brief investigation of parameter sensitivity suggests that the selection of parameters and their range of perturbations appear suitable for a robust correlation analysis. Simultaneous perturbations of multiple parameters are not considered in the present study, as this would require further tuning and calibration of perturbation magnitudes and would thus add to the complexity of the investigation. This remains to be the focus of a future study.

Regression models are constructed to estimate initial SST and MLD perturbations within the vortex using various atmospheric metrics as independent variables. In an azimuthally averaged sense, these models capture about 70% of total variance for SST and up to 55% of total variance for MLD in the hurricane inner core. Furthermore, within the inner core of a hurricane vortex, it is found that storm speed contributes most to upper ocean perturbations (up to 50% variance explained for SST cooling and up to 30% variance explained for MLD perturbation), whereas characteristics of the atmospheric vortex contribute very little. The importance of storm speed in controlling upper ocean perturbations is strongest near the storm center (0–1 RMW), diminishing gradually toward no measurable impact beyond 3 RMW.

The above result compares favorably with the study by Cione et al. (2005), where an algorithm was developed to predict the inner-core SST cooling for the Atlantic basin. That algorithm was based on an observational multivariate regression analysis that demonstrated that storm speed, latitude, and initial SST were the strongest contributors to inner-core SST cooling. The findings of the present study are in agreement in the

0–2 RMW range for storm speed. However, ambient SST does not appear to be a strong contributor here, and no conclusions can be drawn for latitude because of the present study's f -plane assumption. Since latitude and ambient SST are naturally related, one could speculate that the lack of relationship between ambient SST and ocean perturbations in Figure 11 is partially due to the omitted dependence of ambient SST on latitude in the present idealized model configuration. Future iterations of the idealized framework should therefore consider consistently accounting for Coriolis and ambient SST gradients so that a more comprehensive interaction between storm environment and ocean perturbations can be obtained.

The present study's results also have potential consequences for inner-core ocean data assimilation and modeling in general. If a significant portion of the SST cooling and mixed-layer deepening signals is indeed related to storm speed as discussed above, how complex three-dimensional ocean model coupling impacts predictions of intensity change becomes a valid question. One caveat here of course is that the present study only investigates estimation/prediction of upper ocean perturbations in an azimuthally averaged sense and maximum SST cooling thus obtained ranges between 0.5 and 0.9°C for storm speeds of 2–5 m s⁻¹, as opposed to the maximum cooling values of typically greater magnitudes (1–4°C) found in the hurricane wake (Halliwell et al., 2015). This discrepancy is demonstrated in an aggregate sense in Figure 15, where maximum SST cooling anywhere within 100 km of the storm center from all perturbation simulations (Figure 15a) is compared against the azimuthally averaged SST cooling in the same region (Figure 15b). Although the two quantities are strongly correlated ($R = 0.87$), the ratio of maximum-to-mean SST cooling is large, with a narrow frequency distribution and a sharp mode at around 3 (Figure 15c). This indicates that significant and consistent differences exist between larger and smaller wave number components of SST cooling that are also contributed by the lack of a three-dimensional ocean model to simulate the upper ocean thermal structure more realistically. Clearly, further research that employs more complex ocean models is needed to understand the relative contributions of various wave number components of SST cooling to hurricane intensity change.

A planned application of the new atmospheric and ocean initialization schemes is to obtain a realistic idealized hurricane simulation to study model sensitivity to various environment-related and storm-related parameters. It is believed that having established such a control simulation will make it possible to draw conclusions on how actual observed hurricanes should respond to the changes in the factors involved. This remains to be the subject of a future publication.

Acknowledgments

This work was supported in part by NOAA's Hurricane Forecast Improvement Program (HFIP) through the National Weather Service Program Office grant NA12NWS4680010 and was in part carried out under the auspices of CIMAS, a joint institute of the University of Miami and NOAA, cooperative agreement NA15OAR4320064. The data used in the correlation and regression calculations are provided as a supplement along with a readme file that explains data structure. The authors are grateful to Sundararaman Gopalakrishnan for providing an early version of the idealized HWRF model code and to George Halliwell for providing the one-dimensional ocean coupling code for HWRF. Constructive discussions with Vijay Tallapragada and Jian-Wen Bao helped enhance the quality of the numerical simulations presented. Hua Chen and Matthieu Le Henaff from NOAA/AOML provided excellent internal reviews that further improved the manuscript. Comments from two anonymous peer reviewers have helped bring the manuscript to its final form.

References

- Aksoy, A. (2013). Storm-relative observations in tropical cyclone data assimilation with an ensemble Kalman filter. *Monthly Weather Review*, *141*, 506–522. <https://doi.org/10.1175/MWR-D-12-00094.1>
- Aksoy, A., Aberson, S. D., Vukicevic, T., Sellwood, K. J., Lorsolo, S., & Zhang, X. (2013). Assimilation of high-resolution tropical cyclone observations with an ensemble Kalman filter using NOAA/AOML/HRD's HEDAS: Evaluation of the 2008–11 vortex-scale analyses. *Monthly Weather Review*, *141*, 1842–1865. <https://doi.org/10.1175/MWR-D-12-00194.1>
- Bao, J.-W., Gopalakrishnan, S. G., Michelson, S. A., Marks, F. D., & Montgomery, M. T. (2012). Impact of physics representations in the HWRF on simulated hurricane structure and pressure–wind relationships. *Monthly Weather Review*, *140*, 3278–3299. <https://doi.org/10.1175/MWR-D-11-00332.1>
- Barnes, S. L. (1964). A technique for maximizing details in numerical weather map analysis. *Journal of Applied Meteorology*, *3*, 396–409. [https://doi.org/10.1175/1520-0450\(1964\)003<0396:ATFMDI>2.0.CO;2](https://doi.org/10.1175/1520-0450(1964)003<0396:ATFMDI>2.0.CO;2)
- Bender, M. A., Ginis, I., Tuleya, R., Thomas, B., & Marchok, T. (2007). The operational GFDL Coupled Hurricane–Ocean Prediction System and a summary of its performance. *Monthly Weather Review*, *135*, 3965–3989. <https://doi.org/10.1175/2007MWR2032.1>
- Bryan, G. H. (2012). Effects of surface exchange coefficients and turbulence length scales on the intensity and structure of numerically simulated hurricanes. *Monthly Weather Review*, *140*, 1125–1143. <https://doi.org/10.1175/MWR-D-11-00231.1>
- Bryan, G. H., & Rotunno, R. (2009a). Evaluation of an analytical model for the maximum intensity of tropical cyclones. *Journal of the Atmospheric Sciences*, *66*, 3042–3060. <https://doi.org/10.1175/2008MWR2709.1>
- Bryan, G. H., & Rotunno, R. (2009b). The maximum intensity of tropical cyclones in axisymmetric numerical model simulation. *Monthly Weather Review*, *137*, 1770–1789. <https://doi.org/10.1175/2008MWR2709.1>
- Cione, J., Kaplan, J., Gentemann, C., & DeMaria, M. (2005). *Developing an inner-core SST cooling predictor for use in SHIPS* (JHT Final Progress Report). Miami, FL: National Hurricane Center. Retrieved from http://www.nhc.noaa.gov/jht/2003-2005reports/ICSSTCione_JHTfinalreport.pdf
- Cione, J. J., Kalina, E. A., Zhang, J. A., & Uhlhorn, E. W. (2013). Observations of air–sea interaction and intensity change in hurricanes. *Monthly Weather Review*, *141*, 2368–2382. <https://doi.org/10.1175/MWR-D-12-00070.1>
- Cione, J. J., & Uhlhorn, E. W. (2003). Sea surface temperature variability in hurricanes: Implications with respect to intensity change. *Monthly Weather Review*, *131*, 1783–1796. <https://doi.org/10.1175/2562.1>
- Dunion, J. P. (2011). Rewriting the climatology of the tropical North Atlantic and Caribbean Sea atmosphere. *Journal of Climate*, *24*, 893–908. <https://doi.org/10.1175/2010JCLI3496.1>
- Dunion, J. P., & Marron, C. S. (2008). A reexamination of the Jordan mean tropical sounding based on awareness of the Saharan Air Layer: Results from 2002. *Journal of Climate*, *21*, 5242–5233. <https://doi.org/10.1175/2008JCLI1868.1>

- Durden, S. L. (2013). Observed tropical cyclone eye thermal anomaly profiles extending above 300 hPa. *Monthly Weather Review*, *141*, 4256–4268. <https://doi.org/10.1175/MWR-D-13-00021.1>
- Emanuel, K. A. (1995). Sensitivity of tropical cyclones to surface exchange coefficients and a revised steady-state model incorporating eye dynamics. *Journal of the Atmospheric Sciences*, *52*, 3969–3976. [https://doi.org/10.1175/1520-0469\(1995\)052<3969:SOTCTS>2.0.CO;2](https://doi.org/10.1175/1520-0469(1995)052<3969:SOTCTS>2.0.CO;2)
- Ferrier, B. S., Jin, Y., Lin, Y., Black, T., Rogers, E., & DiMego, G. (2002). *Implementation of a new grid-scale cloud and precipitation scheme in the NCEP Eta model*. Paper presented at 19th Conference on Weather Analysis and Forecasting/15th Conference on Numerical Weather Prediction, San Antonio, TX, American Meteor. Society. Retrieved from https://ams.confex.com/ams/SLS_WAF_NWP/techprogram/paper_47241.htm
- Frank, W. M., & Ritchie, E. A. (1999). Effects of environmental flow upon tropical cyclone structure. *Monthly Weather Review*, *127*, 2044–2061. [https://doi.org/10.1175/1520-0493\(1999\)127<2044:EOEFUT>2.0.CO;2](https://doi.org/10.1175/1520-0493(1999)127<2044:EOEFUT>2.0.CO;2)
- Frank, W. M., & Ritchie, E. A. (2001). Effects of vertical wind shear on hurricane intensity and structure. *Monthly Weather Review*, *129*, 2249–2269. [https://doi.org/10.1175/1520-0493\(2001\)129<2249:EOVWSO>2.0.CO;2](https://doi.org/10.1175/1520-0493(2001)129<2249:EOVWSO>2.0.CO;2)
- Ginin, I. (2002). Tropical cyclone–ocean interactions. In W. A. Perrie (Ed.), *Atmosphere–ocean interactions, advances in fluid mechanics series* (Vol. I, No. 33, pp. 83–114). Ashurst, UK: WIT Press.
- Gopalakrishnan, S. G., Marks, F., Jr., Zhang, J. A., Zhang, X., Bao, J.-W., & Tallapragada, V. (2013). A study of the impacts of vertical diffusion on the structure and intensity of the tropical cyclones using the high-resolution HWRF system. *Journal of the Atmospheric Sciences*, *70*, 524–541. <https://doi.org/10.1175/JAS-D-11-0340.1>
- Gopalakrishnan, S. G., Zhang, X., Bao, J.-W., Yeh, K.-S., & Atlas, R. (2011). The experimental HWRF system: A study on the influence of horizontal resolution on the structure and intensity changes in tropical cyclones using an idealized framework. *Monthly Weather Review*, *139*, 1762–1784. <https://doi.org/10.1175/2010MWR3535.1>
- Hakim, G. J. (2011). The mean state of axisymmetric hurricanes in statistical equilibrium. *Journal of the Atmospheric Sciences*, *68*, 1364–1376. <https://doi.org/10.1175/2010JAS3644.1>
- Halliwel, G. R., Jr. (2004). Evaluation of vertical coordinate and vertical mixing algorithms in the HYbrid-Coordinate Ocean Model (HYCOM). *Ocean Modelling*, *7*, 285–322. <https://doi.org/10.1016/j.ocemod.2003.10.002>
- Halliwel, G. R., Jr., Gopalakrishnan, S., Marks, F., & Willey, D. (2015). Idealized study of ocean impacts on tropical cyclone intensity forecasts. *Monthly Weather Review*, *143*, 1142–1165. <https://doi.org/10.1175/MWR-D-14-00022.1>
- Haus, B. K., Jeong, D., Donelan, M. A., Zhang, J. A., & Savelyev, I. (2010). Relative rates of sea-air heat transfer and frictional drag in very high winds. *Geophysical Research Letters*, *37*, L07802. <https://doi.org/10.1029/2009GL042206>
- Hawkins, H. F., & Imbembo, S. M. (1976). The structure of a small, intense hurricane—Inez 1966. *Monthly Weather Review*, *104*, 418–442. [https://doi.org/10.1175/1520-0493\(1976\)104<0418:TSOASI>2.0.CO;2](https://doi.org/10.1175/1520-0493(1976)104<0418:TSOASI>2.0.CO;2)
- Hawkins, H. F., & Rubsam, D. T. (1968). Hurricane Hilda, 1964. *Monthly Weather Review*, *96*, 617–636. [https://doi.org/10.1175/1520-0493\(1968\)096<0701:HH>2.0.CO;2](https://doi.org/10.1175/1520-0493(1968)096<0701:HH>2.0.CO;2)
- Hong, S.-Y., & Pan, H.-L. (1998). Convective trigger function for a mass-flux cumulus parameterization scheme. *Monthly Weather Review*, *126*, 2599–2620. [https://doi.org/10.1175/1520-0493\(1998\)126<2599:CTFFAM>2.0.CO;2](https://doi.org/10.1175/1520-0493(1998)126<2599:CTFFAM>2.0.CO;2)
- Hsu, S. A., & Yan, Z. (1998). A note on the radius of maximum wind for hurricanes. *Journal of Coastal Research*, *14*, 667–668.
- Jordan, C. L. (1958). Mean soundings for the West Indies area. *Journal of Meteorology*, *15*, 91–97. [https://doi.org/10.1175/1520-0469\(1958\)015<0091:MSFTWI>2.0.CO;2](https://doi.org/10.1175/1520-0469(1958)015<0091:MSFTWI>2.0.CO;2)
- Keptert, J. (2001). The dynamics of boundary layer jets within the tropical cyclone core. Part I: Linear theory. *Journal of the Atmospheric Sciences*, *58*, 2469–2484. [https://doi.org/10.1175/1520-0469\(2001\)058<2469:TDOBL>2.0.CO;2](https://doi.org/10.1175/1520-0469(2001)058<2469:TDOBL>2.0.CO;2)
- Landsea, C. W., & Franklin, J. L. (2013). Atlantic hurricane database uncertainty and presentation of a new database format. *Monthly Weather Review*, *141*, 3576–3592. <https://doi.org/10.1175/MWR-D-12-00254.1>
- LaSeur, N. E., & Hawkins, H. F. (1963). An analysis of Hurricane Cleo (1958) based on data from research reconnaissance aircraft. *Monthly Weather Review*, *91*, 694–709. [https://doi.org/10.1175/1520-0493\(1963\)091<0694:AAOHC>2.3.CO;2](https://doi.org/10.1175/1520-0493(1963)091<0694:AAOHC>2.3.CO;2)
- Lin, I.-I., Gustavo, J. G., Knaff, J. A., Forbes, C., & Ali, M. M. (2013). Ocean heat content for tropical cyclone intensity forecasting and its impact on storm surge. *Natural Hazards*, *66*, 1481–1500. <https://doi.org/10.1007/s11069-012-0214-5>
- Lorsolo, S., & Aksoy, A. (2012). Wavenumber analysis of azimuthally distributed data: Assessing maximum allowable gap size. *Monthly Weather Review*, *140*, 1945–1956. <https://doi.org/10.1175/MWR-D-11-00219.1>
- Nguyen, V. S., Smith, R. K., & Montgomery, M. T. (2008). Tropical-cyclone intensification and predictability in three dimensions. *Quarterly Journal of the Royal Meteorological Society*, *134*, 563–582. <https://doi.org/10.1002/qj.235>
- Nolan, D. S. (2011). Evaluating environmental favorableness for tropical cyclone development with the method of point-downscaling. *Journal of Advances in Modeling Earth Systems*, *3*, M08001. <https://doi.org/10.1029/2011MS000063>
- Nolan, D. S., Atlas, R., Bhatia, K. T., & Bucci, L. R. (2013). Development and validation of a hurricane nature run using the joint OSSE nature run and the WRF model. *Journal of Advances in Modeling Earth Systems*, *5*, 382–405. <https://doi.org/10.1002/jame.20031>
- Nolan, D. S., & Montgomery, M. T. (2000). The algebraic growth of wavenumber one disturbances in hurricane-like vortices. *Journal of the Atmospheric Sciences*, *57*, 3514–3538. [https://doi.org/10.1175/1520-0469\(2000\)057<3514:TAGOWO>2.0.CO;2](https://doi.org/10.1175/1520-0469(2000)057<3514:TAGOWO>2.0.CO;2)
- Nolan, D. S., Rappin, E. D., & Emanuel, K. A. (2007). Tropical cyclogenesis sensitivity to environmental parameters in radiative–convective equilibrium. *Quarterly Journal of the Royal Meteorological Society*, *133*, 2085–2107. <https://doi.org/10.1002/qj.170>
- Nolan, D. S., Zhang, J. A., & Stern, D. P. (2009). Evaluation of planetary boundary layer parameterizations in tropical cyclones by comparison of in-situ data and high-resolution simulations of Hurricane Isabel (2003). Part I: Initialization, maximum winds, and outer core boundary layer structure. *Monthly Weather Review*, *137*, 3651–3674. <https://doi.org/10.1175/2009MWR2785.1>
- Pan, H.-L., & Wu, J. (1995). *Implementing a mass flux convection parameterization package for the NMC Medium-Range Forecast model* (NMC Off. Note 409, 40 pp.). Washington, DC: NCEP.
- Price, J. (1981). Upper ocean response to a hurricane. *Journal of Physical Oceanography*, *11*, 153–175. [https://doi.org/10.1175/1520-0485\(1981\)011<0153:UORTAH>2.0.CO;2](https://doi.org/10.1175/1520-0485(1981)011<0153:UORTAH>2.0.CO;2)
- Rappin, E. D., & Nolan, D. S. (2012). The effect of vertical shear orientation on tropical cyclogenesis. *Quarterly Journal of the Royal Meteorological Society*, *138*, 1035–1054. <https://doi.org/10.1002/qj.977>
- Rogers, R., Reasor, P., & Lorsolo, S. (2013b). Airborne Doppler observations of the inner-core structural differences between intensifying and steady-state tropical cyclones. *Monthly Weather Review*, *141*, 2970–2991. <https://doi.org/10.1175/MWR-D-12-00357.1>
- Rogers, R. F., Aberson, S., Aksoy, A., Annane, B., Black, M., Cione, J., ... Zhang, X. (2013a). NOAA's hurricane intensity forecasting experiment: A progress report. *Bulletin of the American Meteorological Society*, *94*, 859–882. <https://doi.org/10.1175/BAMS-D-12-00089.1>
- Rogers, R. F., Reasor, P. D., & Zhang, J. A. (2015). Multiscale structure and evolution of Hurricane Earl (2010) during rapid intensification. *Monthly Weather Review*, *143*, 536–562. <https://doi.org/10.1175/MWR-D-14-0>

- Smith, R. B. (1993). A hurricane beta-drift law. *Journal of the Atmospheric Sciences*, *50*, 3213–3215. [https://doi.org/10.1175/1520-0469\(1993\)050<3213:AHBDL>2.0.CO;2](https://doi.org/10.1175/1520-0469(1993)050<3213:AHBDL>2.0.CO;2)
- Smith, R. K., Montgomery, M. T., & Persing, J. (2014). On steady-state tropical cyclones. *Quarterly Journal of the Royal Meteorological Society*, *140*, 2638–2649. <https://doi.org/10.1002/qj.2329>
- Stern, D. P., & Nolan, D. S. (2012). On the height of the warm core in tropical cyclones. *Journal of the Atmospheric Sciences*, *69*, 1657–1680. <https://doi.org/10.1175/JAS-D-11-010.1>
- Tabachnick, B. G., & Fidell, L. S. (2001). Principal components and factor analysis. In *Using multivariate statistics* (4th ed., pp. 582–652). Needham Heights, MA: Allyn and Bacon.
- Tong, M., & Xue, M. (2008). Simultaneous estimation of microphysical parameters and atmospheric state with simulated radar data and ensemble square root Kalman filter. Part I: Sensitivity analysis and parameter identifiability. *Monthly Weather Review*, *136*, 1630–1648. <https://doi.org/10.1175/2007MWR2070.1>
- Uhlhorn, E. W., Klotz, B. W., Vukicevic, T., Reasor, P. D., & Rogers, R. F. (2014). Observed hurricane wind speed asymmetries and relationships to motion and environmental shear. *Monthly Weather Review*, *142*, 1290–1311. <https://doi.org/10.1175/MWR-D-13-00249.1>
- Wang, Y. (1995). An inverse balance equation in sigma coordinates for model initialization. *Monthly Weather Review*, *123*, 482–488. [https://doi.org/10.1175/1520-0493\(1995\)123<0482:AIBEIS>2.0.CO;2](https://doi.org/10.1175/1520-0493(1995)123<0482:AIBEIS>2.0.CO;2)
- Zawislak, J., Jiang, H., Alvey, G. R., III, Zipser, E. J., Rogers, R. F., Zhang, J. A., & Stevenson, S. N. (2015). Observations of the structure and evolution of Hurricane Edouard (2014) during intensity change. Part I: Relationship between the thermodynamic structure and precipitation. *Monthly Weather Review*, *144*, 3333–3354. <https://doi.org/10.1175/MWR-D-16-0018.1>
- Zhang, D.-L., & Chen, H. (2012). Importance of the upper-level warm core in the rapid intensification of a tropical cyclone. *Geophysical Research Letters*, *39*, L02806. <https://doi.org/10.1029/2011GL050578>
- Zhang, D.-L., Zhu, L., Zhang, X., & Tallapragada, V. (2015). Sensitivity of idealized hurricane intensity and structures under varying background flows and initial vortex intensities to different vertical resolutions in HWRF. *Monthly Weather Review*, *143*, 914–932. <https://doi.org/10.1175/MWR-D-14-00102.1>
- Zhang, F., & Tao, D. (2013). Effects of vertical wind shear on the predictability of tropical cyclones. *Journal of the Atmospheric Sciences*, *70*, 975–983. <https://doi.org/10.1175/JAS-D-12-0133.1>
- Zhang, J. A. (2010). Estimation of dissipative heating using low-level in-situ aircraft observations in the hurricane boundary layer. *Journal of the Atmospheric Sciences*, *67*, 1853–1862. <https://doi.org/10.1175/2010JAS3397.1>
- Zhang, J. A., & Drennan, W. M. (2012). An observational study of vertical eddy diffusivity in the hurricane boundary layer. *Journal of the Atmospheric Sciences*, *69*, 3223–3236. <https://doi.org/10.1175/JAS-D-11-0348.1>
- Zhang, J. A., Nolan, D. S., Rogers, R. F., & Tallapragada, V. (2015). Evaluating the impact of improvements in the boundary layer parameterization on hurricane intensity and structure forecasts in HWRF. *Monthly Weather Review*, *143*, 3136–3155. <https://doi.org/10.1175/MWR-D-14-00339.1>
- Zhang, J. A., Rogers, R. F., Nolan, D. S., & Marks, F. D. (2011). On the characteristic height scales of the hurricane boundary layer. *Monthly Weather Review*, *139*, 2523–2535. <https://doi.org/10.1175/MWR-D-10-05017.1>
- Zhang, J. A., & Uhlhorn, E. W. (2012). Hurricane sea surface inflow angle and an observation-based parametric model. *Monthly Weather Review*, *140*, 3587–3605. <https://doi.org/10.1175/MWR-D-11-00339.1>